

# Toward a Unified Mechanism for Oxoammonium Salt-Mediated Oxidation Reactions: A Theoretical and Experimental Study Using a Hydride Transfer Model

Trevor A. Hamlin,<sup>†,||</sup> Christopher B. Kelly,<sup>†,||</sup> John M. Ovian,<sup>†</sup> Rebecca J. Wiles,<sup>†</sup> Leon J. Tilley,<sup>‡</sup> and Nicholas E. Leadbeater<sup>\*,†,§</sup>

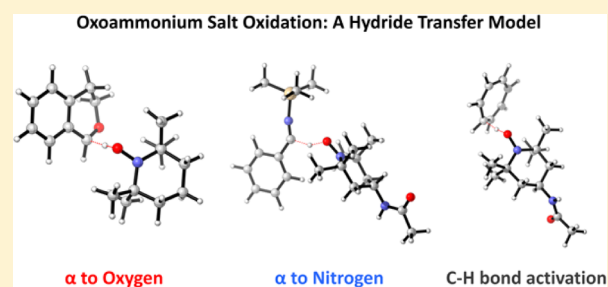
<sup>†</sup>Department of Chemistry, University of Connecticut, 55 North Eagleville Road, Storrs, Connecticut 06269, United States

<sup>‡</sup>Department of Chemistry, Stonehill College, 320 Washington Street, Easton, Massachusetts 02357, United States

<sup>§</sup>Department of Community Medicine & Health Care, University of Connecticut Health Center, The Exchange, 263 Farmington Avenue, Farmington, Connecticut 06030, United States

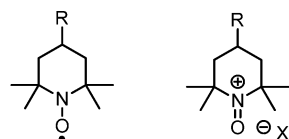
## Supporting Information

**ABSTRACT:** A range of oxoammonium salt-based oxidation reactions have been explored computationally using density functional theory (DFT), and the results have been correlated with experimentally derived trends in reactivity. Mechanistically, most reactions involve a formal hydride transfer from an activated C–H bond to the oxygen atom of the oxoammonium cation. Several new potential modes of reactivity have been uncovered and validated experimentally.



## 1. INTRODUCTION

Oxidation is one of the most important and fundamental transformations in synthetic organic chemistry.<sup>1</sup> Consequently, many reagents have been developed to accomplish oxidations in an effective and selective manner. Among known oxidizing reagents, those based on oxoammonium cations, especially oxidants bearing the 2,2,6,6-tetramethylpiperidyl scaffold (Figure 1), have found wide applicability because of their versatility,



X:  $\text{Cl}^-$ ,  $\text{Br}^-$ ,  $\text{NO}_3^-$ ,  $\text{ClO}_4^-$ ,  $\text{BF}_4^-$ ,  $\text{PF}_6^-$  etc.  
R: H, OMe, OH, =O, NHAc etc.

**Figure 1.** Common 2,2,6,6-tetramethylpiperidine-based nitroxides and oxoammonium salts.

selectivity, and mildness.<sup>2,3</sup> Oxoammonium cations can be generated *in situ* by a single electron transfer (SET) to a terminal oxidant and subsequently employed for catalytic oxidation. Alternatively, oxidations can be conducted stoichiometrically using oxoammonium salts.<sup>2,3</sup> Both approaches have been employed in the oxidation of an array of functional groups including alcohols, amines, and aldehydes.<sup>2–5</sup> The catalytic approach is frequently exploited for industrial scale oxidation.<sup>6</sup>

A majority of reports involving 2,2,6,6-tetramethylpiperidine 1-oxyl based (TEMPO) catalysts or 2,2,6,6-tetramethylpiper-

idine-1-oxoammonium-based salts ( $\text{TEMP}=\text{O}^+ \text{X}^-$ ) center on the oxidation of alcohols to their corresponding carbonyl species.<sup>2</sup> This application is not surprising given the ubiquity of this type of functional group interconversion in organic synthesis. Early mechanistic studies by Semmelhack et al. concluded that the mechanism of this transformation involved nucleophilic attack on the positive nitrogen of the oxoammonium cation by an alkoxide, followed by an intramolecular E2-like elimination (see I in Figure 2).<sup>7</sup> This is by far the prevailing mechanism reported in the literature but seems counterintuitive given the severe steric constraints of the nitrogen atom in this scaffold.<sup>2,5a</sup> Indeed, even in this seminal report, Semmelhack et al. note that carbon nucleophiles attack solely at the oxygen. The

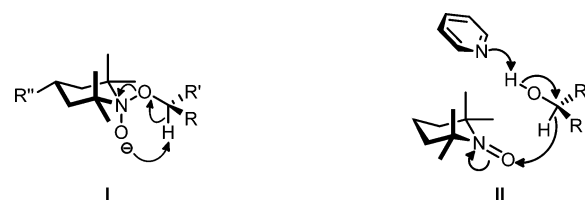


**Figure 2.** Possible avenues for oxidation using 2,2,6,6-tetramethylpiperidine-based oxoammonium cations. (I) Key species proposed by Semmelhack et al.<sup>7</sup> (II) Our previously proposed hydride transfer based model for the base-assisted oxidation of methanol using the TEMPO-based oxoammonium cation.

Received: June 2, 2015

Published: July 13, 2015

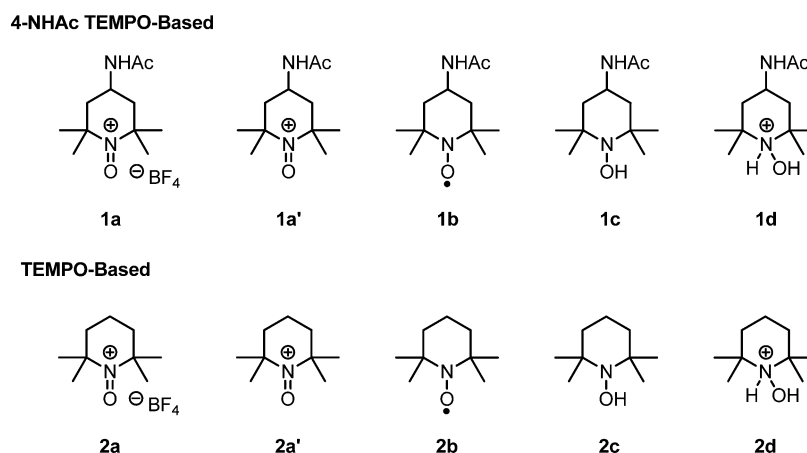


**Figure 3.** Oxoammonium cations and salts as well as related species discussed in this paper.

question, therefore, arises as to why other nucleophiles would behave differently.

Recently, members of our team suggested that the primary mode of operation of these cations is as though the positive charge is on the oxygen atom of the oxoammonium salt, effectively giving rise to an electrophilic, hydride-accepting oxygen.<sup>8</sup> From this standpoint, a mechanism originally ruled out by Semmelhack becomes far more viable, namely, one involving a hydride transfer from an activated C–H bond to the electrophilic oxygen of the oxoammonium cation.

Bailey et al. have recently probed the oxidation of alcohols under neutral and basic conditions using computational modeling.<sup>9</sup> In their report, they invoked a hydride transfer under neutral conditions, whereas, under basic conditions, they argued for a complex similar to the one proposed by Semmelhack et al.<sup>7,9</sup> Building on this work, members of our group, in conjunction with Bobbitt et al., further investigated the mechanism of oxoammonium salt oxidations of methanol under non-base-assisted and pyridyl-base-assisted conditions.<sup>8</sup> This study suggested that a hydride transfer model was actually plausible in both cases. We then wondered whether this mechanism was at play not only for the oxidation of alcohols but also for a number of other oxidation reactions mediated by 2,2,6,6-tetramethylpiperidine-based oxoammonium salts. We, therefore, decided to use computational and experimental methods to probe a variety of oxidative transformations reported previously by us and others involving these salts. Additionally, we sought to further explore the intricacies of the oxidation of alcohols under unassisted and base-assisted conditions, as well as use our results as a predictive tool for the feasibility of yet unreported oxidations. The results of this combined experimental and computational endeavor are reported herein.

## 2. RESULTS AND DISCUSSION

Our analysis is broken down into three parts based on the substituents around the C–H bond being oxidized: (1) at C–H bonds  $\alpha$  to oxygen, (2) at C–H bonds  $\alpha$  to nitrogen, and (3) at C–H bonds without any heteroatom assistance (C–H bond activation). Experimental evidence and computationally derived models are reported in these sections. Quantum chemical calculations were performed using Gaussian 09.<sup>10</sup> The method used for the calculations of nonmetal containing systems involves (i) geometry optimization and vibrational frequency calculations in implicit dichloromethane ( $\text{CH}_2\text{Cl}_2$ ) or acetonitrile (MeCN) using CPCM<sup>11</sup> at the DFT(B3LYP)/6-31+G(d) level of

theory<sup>12,13</sup> and (ii) single-point solvation free energy calculation in  $\text{CH}_2\text{Cl}_2$  or MeCN using CPCM with DFT(B3LYP)//6-311++G(d,p). The method used for the calculations of iron containing systems involves (i) geometry optimization and vibrational frequency calculations in implicit  $\text{CH}_2\text{Cl}_2$  or MeCN using CPCM at the DFT(B3LYP/LANL2DZ)<sup>14</sup> level of theory for iron and DFT(B3LYP)/6-31+G(d) level of theory for the rest of the atoms and (ii) single-point solvation free energy calculation in  $\text{CH}_2\text{Cl}_2$  or MeCN using CPCM with DFT-(B3LYP/SDD)<sup>15</sup> for iron and DFT(B3LYP)/6-311++G(d,p) for all other atoms. Gibbs free energies in solution are obtained by adding the thermal correction to the Gibbs free energy from (i) to the solvation electronic energy calculated in (ii). Radical species were treated in an analogous fashion as described above for closed-shell systems; however, unrestricted calculations were employed. Stationary points were characterized by frequency calculations at 298 K, with structures at energy minima showing no imaginary frequencies and transition-state structures showing one imaginary frequency. All calculations were carried out at 298 K and 1 atm, and the concentration was 1 M. Intrinsic reaction coordinate (IRC) calculations followed by optimization and frequency calculations were performed to unambiguously connect transition-state structures with associated reactants and products along the reaction coordinate.<sup>16</sup> All energy values shown are in  $\text{kcal mol}^{-1}$ , bond lengths are reported in angstroms (Å), and bond angles in degrees ( $^\circ$ ). Molecular figures were generated using CYLView.<sup>17</sup>

Two families of 2,2,6,6-tetramethylpiperidine oxoammonium ions have been studied computationally in this report. Additionally, two different oxoammonium salts that have been used in experimental studies performed by us and others will be discussed. For clarity, these various species are presented in Figure 3, along with their respective compound numbers.

### 2.1. Oxidations $\alpha$ to Oxygen. 2.1.1. Alcohol Oxidation.

Given that oxoammonium salts are primarily used for the routine oxidation of alcohols to aldehydes, we initially focused our efforts on exploring the details of this transformation.<sup>4,5</sup> In addition, these reactions have been the subject of preliminary studies by us and members of our team.<sup>8</sup> We hypothesized that a fundamental understanding of this type of oxidation would be instrumental in elucidating the key features governing other oxidation reactions  $\alpha$  to oxygen.

We began by using benzyl alcohol as a representative substrate to probe the differences between the unassisted and base-assisted oxidation. While we had evaluated this in our past report in the

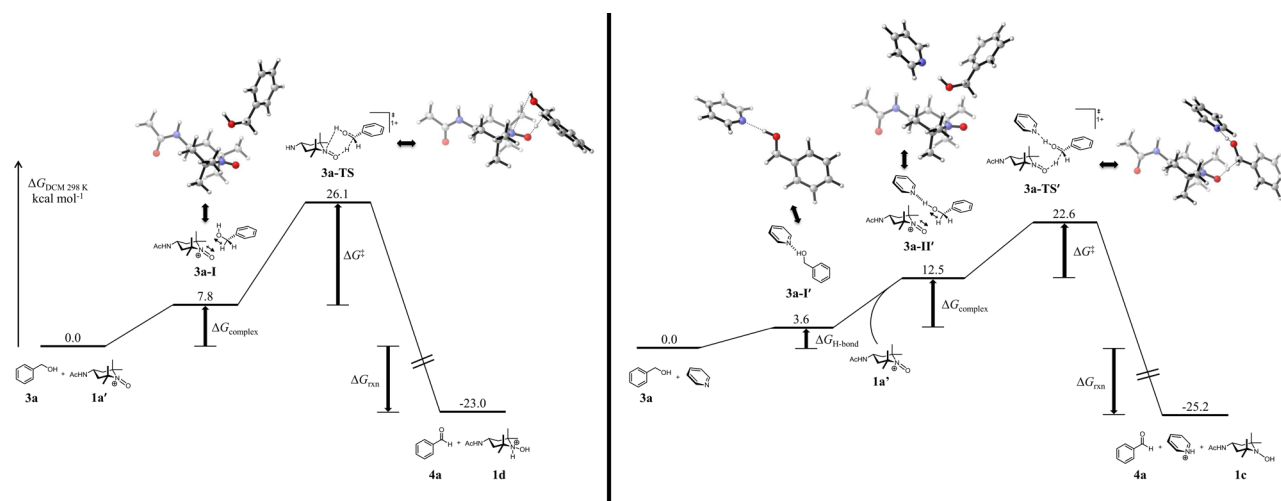


**Figure 4.** Disparate mechanistic pathways for the oxidation of benzyl alcohol. The reaction profile on the left represents the unassisted mechanism, while that on the right is the base-assisted process. Values are in kcal mol<sup>-1</sup>.

**Table 1. Energetics of Alcohol Oxidation in the Unassisted Mechanism for Various Substrates**

Entry	Alcohol (3)	$\Delta G_{\text{complex}}$ (3 to 3-I) <sup>a</sup>	$\Delta G^{\ddagger}$ (3-I to 3-TS) <sup>a</sup>	Rel. Reactivity <sup>b</sup>
1		7.8	18.3	1.0
2		7.8	13.1	4.8
3		7.8	20.0	0.61
4		8.4	17.5	0.64
5		9.1	19.3	0.20
6		8.5	21.9	0.10
7		7.5	13.2	5.3
8		9.4	20.0	0.03
9		9.9	18.2	0.06
10		8.8	23.4	0.01
11		5.5	29.6	0.0
12		7.6	32.1	0.0
13		6.7	39.5	0.0

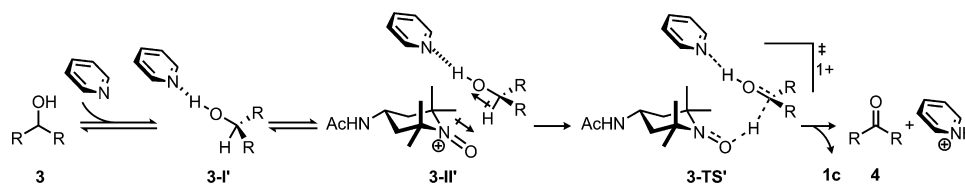
<sup>a</sup>Values in kcal mol<sup>-1</sup>. <sup>b</sup>Experimentally obtained values from competitive studies

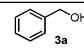
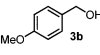
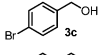
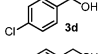
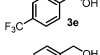
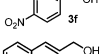
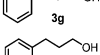
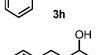
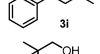
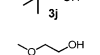
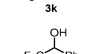
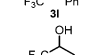
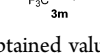
theoretical oxidation of methanol, there are two key differences in this contribution: (1) we invoke the formation of a dipole-stabilized preoxidation complex between the oxidant and the alcohol, and (2) we use 1a' itself rather than 2a'. The formation of a dipole-stabilized preoxidation complex is predicated on recent computational studies by Wiberg and co-workers focused around the oxidation of amines to nitriles,<sup>18</sup> while use of 1a' itself improves the overall accuracy of our modeling. Using the results

of this study, we were able to construct the potential energy surface for both reaction types (Figure 4).

In the case of the non-base-assisted mechanism (Figure 4, left), we observed a concerted, but asynchronous, oxidation event where the primary molecular motion in the transition-state structure is that of the hydride transfer from the alcohol to the electrophilic oxygen of 1a', followed by a proton transfer to the now basic nitrogen of the resulting hydroxylamine 1c, generating 1d and the aldehyde. These two distinct events can be observed

Table 2. Energetics of Alcohol Oxidation in the Base-Assisted Mechanism for Various Substrates



Entry	Alcohol (3)	$\Delta G_{\text{H-bond}}$ (3 to 3-I') <sup>a</sup>	$\Delta G_{\text{Complex}}$ (3-I to 3-II') <sup>a</sup>	$\Delta G^\ddagger$ (3-II' to 3-TS') <sup>a</sup>	Rel. React. <sup>b</sup>
1		3.6	9.0	9.9	1.0
2		4.5	8.4	7.5	1.3
3		4.1	8.7	12.6	0.83
4		3.9	8.2	12.4	0.85
5		3.6	9.3	12.6	0.78
6		2.9	10.5	12.2	0.77
7		4.0	7.4	8.4	2.1
8		5.2	7.1	13.4	0.62
9		6.8	8.5	14.1	0.12
10		4.4	10.2	13.3	0.0
11		3.6	8.5	13.8	- <sup>c</sup>
12		2.2	11.4	14.9	0.0
13		2.5	8.7	18.4	0.0

<sup>a</sup>Values in kcal mol<sup>-1</sup>. <sup>b</sup>Experimentally obtained values from competitive studies. <sup>c</sup>Not assessed due to propensity of product to undergo oxidative esterification; see ref 8.

when performing intrinsic reaction coordinate (IRC) calculations (see the SI for IRC plots). The  $\Delta G^\ddagger$  value from the preoxidation complex is reasonable (18.3 kcal mol<sup>-1</sup>), and the overall reaction is thermodynamically favorable. The required energy to reach the preoxidation complex ( $\Delta G_{\text{complex}}$ ) is a consequence of a more organized state, and the pathway has a  $\Delta S_{\text{complex}} = -0.030$  kcal mol<sup>-1</sup> K<sup>-1</sup>.

In the base-assisted mechanism, we presupposed the formation of a hydrogen-bonding complex (energetically defined as  $\Delta G_{\text{H-bond}}$ ) between benzyl alcohol and pyridine based on experimental evidence garnered in our previous report.<sup>8</sup> We then assumed the likely reversible formation of a dipole-stabilized preoxidation complex. Not surprisingly, the overall change in energy to reach this even more entropically demanding state ( $\Delta S_{\text{complex}} = -0.037$  kcal mol<sup>-1</sup> K<sup>-1</sup>) was higher as compared to the unassisted mechanism (7.8 kcal mol<sup>-1</sup> for  $\Delta G_{\text{complex}}$  in the unassisted mechanism vs 8.9 kcal mol<sup>-1</sup> for  $\Delta G_{\text{complex}}$  from the hydrogen-bonded complex). While this mechanism is similarly highly favorable thermodynamically to the unassisted mechanism, the  $\Delta G^\ddagger$  value for the preoxidation complex is substantially lower (10.1 kcal mol<sup>-1</sup>). This explains the significant rate acceleration observed for the base-assisted mechanism.<sup>8</sup>

With these potential energy surfaces in hand, we sought to evaluate factors governing oxidation in both mechanistic pathways, namely, (i) the disparity between unassisted and base-assisted oxidation, (ii) the role of electronics in this

oxidation process, and (iii) the overall nature of the oxidation (concerted or otherwise). To do this, we modeled the oxidation of numerous alcohols with varying steric and electronic environments. The results of these studies are shown in Tables 1 and 2. Also included in these studies are our experimental relative reactivities of alcohols in oxoammonium salt oxidation. Using these data, we were able not only to elucidate some interesting trends but also to provide some commentary on the limitations of relative-reactivities studies in this type of reaction.

Steric and electronic interactions appear to have a noticeable effect on the ability to form the requisite dipole-stabilized complex. However, the effect is somewhat complex. Distant electron-withdrawing groups (EWGs) or sterically demanding environments deter complexation (Table 1, entries 4–6, 9, and 10), whereas nearby EWGs appear to favor complexation (Table 1, entries 11–13). We quickly ascertained that, while the experimentally derived relative reactivities are mostly a function of the  $\Delta G^\ddagger$  of oxidation, the  $\Delta G_{\text{complex}}$  also plays a role. Alcohols with near-identical activation barriers but with disparate energies of complexation have differing reactivity values (e.g., entries 2 and 7 or entries 1 and 8). In this case, the concentration of the pre-equilibrium complex could be the controlling factor. The lower energy complex would be higher in concentration in solution and thus limit the availability of 1a/1a' to oxidize any other competing alcohol. In turn, this would result in a disparity

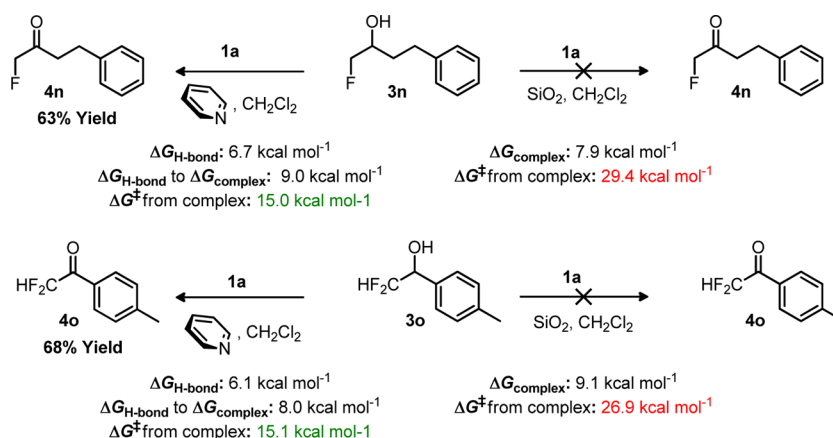


**Figure 5.** Comparison of the theoretical and experimental oxidation of  $\alpha$ - $\text{CH}_2\text{F}$  and  $\alpha$ - $\text{CF}_2\text{H}$  alcohols in the base and non-base-assisted mechanisms.

in the experimental relative reactivities (which are obtained from competition studies) of two alcohols.

In the non-base-assisted mechanism,  $\Delta G^\ddagger$  is most certainly a function of the stability of the forming oxonium-like ion. This trend is apparent when comparing the effect EWGs and electron-donating groups (EDGs) have on alcohols of near-identical steric environments (Table 1, entries 1–6). Alcohols with significant substitution and those that are more apt to participate in resonance-stabilization have lower overall activation barriers. Inductively destabilizing groups can negate the benefits of substitution and dramatically raise  $\Delta G^\ddagger$ . Severely sterically encumbered alcohols also have higher activation barriers, likely due to steric repulsion (entries 9–13, Table 1).

Using these same alcohols, we probed the energetic differences and trends in the base-assisted mechanism. The results of this study are shown in Table 2. Two trends become immediately apparent: (1) The magnitude of  $\Delta G^\ddagger$  (from the dipole stabilized complex) is about half that of the analogous non-base-assisted  $\Delta G^\ddagger$  value, and (2) the energy required to form the preoxidation complex is very close to that needed for the hydride transfer event (though the magnitude of each value is independent of one another). Taken together, this implies that oxidation should proceed rapidly and the oxidation should be less sensitive to electronic perturbations. This is indeed the case experimentally. Oxidations under base-assisted conditions proceed much faster at room temperature ( $\approx 1$ – $2$  h on average) as compared to analogous unassisted oxidations ( $\approx 6$ – $48$  h).<sup>4,8</sup> Additionally, the relative reactivities reflect a relative insensitivity to alcohol structure.

Subtle trends are also apparent. The value of  $\Delta G_{\text{H-bond}}$  appears to be a function of alcohol acidity. This explains the less uniform  $\Delta G_{\text{complex}}$  values for benzyl alcohols with varying electronic, yet identical, steric environments. As in the unassisted mechanism,  $\Delta G_{\text{complex}}$  is mostly a function of steric interactions. As noted in our previous report, the value of  $\Delta G_{\text{H-bond}}$  is also a function of the basicity of the pyridyl base.<sup>8</sup> Since this mechanism involves a more sterically (and entropically) demanding complex, the values for complexation are, on a whole, larger than in the unassisted mechanism. While the relative reactivities are influenced by the respective values of  $\Delta G_{\text{H-bond}}$  and  $\Delta G_{\text{complex}}$ , the overriding measure of reaction success is  $\Delta G^\ddagger$  from the dipole-stabilized complex.

As a means to use the data collected in a predictive manner, we computed the energies of oxidation of two classes of alcohols that have not been subjected to oxoammonium salt oxidations,

namely,  $\alpha$ -fluoromethyl (3n) and  $\alpha$ -difluoromethyl (3o) substrates (Figure 5). Specifically, we examined an aliphatic fluoromethyl alcohol and a benzyl difluoromethyl alcohol. On the basis of their respective computed values for  $\Delta G^\ddagger$  and  $\Delta G_{\text{complex}}$  in the unassisted mechanism, one would expect both alcohols to fail to oxidize. Experimental results confirmed this prediction. Also, a tentative cutoff value for  $\Delta G^\ddagger$  between successful and unsuccessful unassisted oxidation at room temperature was determined by this analysis. This barrier must lie between 23.4 and 29.6 kcal mol<sup>-1</sup> (most likely closer to the lower end of the range given the lower relative reactivity of 3j in Table 1). We performed a similar calculation using the base-assisted mechanism. The computed values of  $\Delta G^\ddagger$  suggested that both would be readily oxidized, and this was indeed the case experimentally. The cutoff for oxidation in the base-assisted mechanism at room temperature is likely around 15.0–18.4 kcal mol<sup>-1</sup> based on these results and those for entries 12 and 13 of Table 2.

**2.1.2. Oxidation of Ethers.** In 2009, Bailey and co-workers reported that benzyl ethers could be oxidatively cleaved under mild conditions in the presence of 1a (Figure 6).<sup>19</sup> In the original report by these authors, the posited mechanism hinged on a formal hydride transfer.

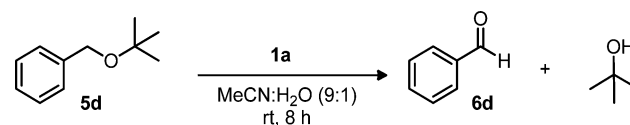


**Figure 6.** Example of the oxidative cleavage of benzyl ethers reported by Bailey and co-workers.<sup>19</sup>

To continue our investigation of oxidations at alkyl groups  $\alpha$  to oxygen, we explored the theoretical oxidation of methyl benzyl ether (5a) computationally, using our previous findings with alcohols as a guide (Figure 7). However, unlike the case of the alcohols, a preoxidation complex was not preferable given the new steric constraints of the methyl group attached to the oxygen (confirmed by IRC calculations). Thus, we modeled the mechanism without the formation of such a complex. Interestingly, the  $\Delta G^\ddagger$  was markedly lower for 5a as compared to benzyl alcohol (3a). While this may be due to electronic differences between the oxygen atom in the two cases, it more likely results from modeling the reaction in a more polar solvent ( $\text{CH}_2\text{Cl}_2$  for benzyl alcohol vs  $\text{MeCN}$  for benzyl ether). However, given that these oxidative cleavage processes mediated

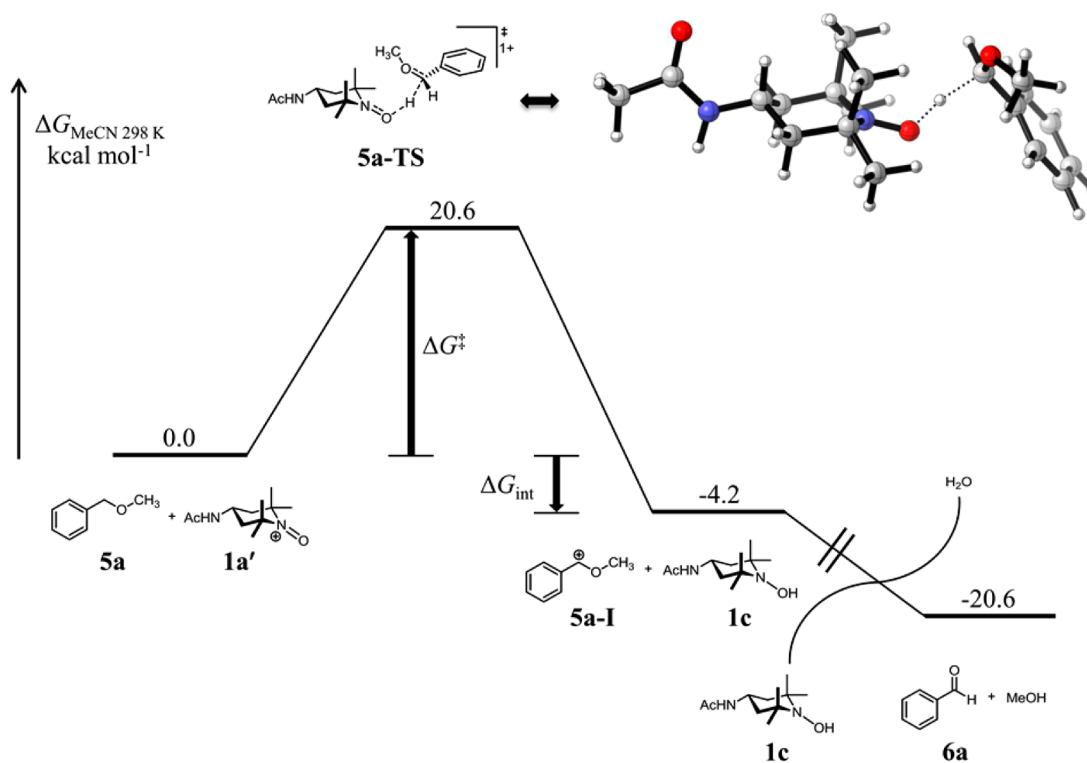


Figure 7. Computed reaction profile for the oxidation of methyl benzyl ether to benzaldehyde mediated by 1a'.

Table 3. Energetics of Benzyl Ether Cleavage Facilitated by 1a'

Entry	Benzyl Ether	$\Delta G^\ddagger$ (5 to 5-TS) <sup>a</sup>	$\Delta G_{\text{int}}$ (5 to 5-I) <sup>a</sup>	$\Delta\Delta G_{\text{int}}$ <sup>a,b</sup>
1		30.6	-4.2	0
2		30.7	-5.9	-0.9
3		31.9	-5.1	-1.7
4		36.5	-8.6	-4.4
5		35.0	1.4	5.6
6		28.3	-11.0	-6.7
7		32.2	-3.3	0.9
8		36.0	3.6	7.9
9		32.0	-10.1	-5.9
10		42.8	4.7	8.9

<sup>a</sup>Values in kcal mol<sup>-1</sup>. <sup>b</sup>Defined as the difference in  $\Delta G_{\text{int}}$  between the current entry and entry 1.

by **1a** are experimentally conducted in acetonitrile, we felt that that using MeCN as the implicit solvent for our solvation model would be more accurate in describing the energetics of this reaction. We were unable to find transition-state structures leading to the hydrolysis of the intermediate oxonium ion, but were able to evaluate both the  $\Delta G_{\text{int}}$  leading to the intermediate oxonium ion as well as the overall  $\Delta G_{\text{rxn}}$ . Both  $\Delta G$  values indicated the processes were favorable and spontaneous.

In addition to modeling this specific reaction, we sought to both reproduce the observed experimental trends and explore other subtle details of this process. To do this, we calculated both the  $\Delta G^\ddagger$  and the  $\Delta G_{\text{int}}$  for a variety of benzyl ether substrates. We wanted to evaluate the possibility that the hydride transfer could be reversible, given that, unlike alcohols, there is no readily accessible way to neutralize the charge of the intermediate oxonium ion and this ion itself may serve as an oxidant. Our results are displayed in Table 3.

More information can be garnered from relative trends from a reference point than from the actual numerical values of the oxidation. This is especially true given the fact that these values are not from a preoxidation complex, but rather from the two isolated species and thus may have artificially high activation barriers. To determine relative trends, we selected benzyl methyl ether (**5a**) as our reference point and studied differences in both the activation energies for the reaction ( $\Delta G^\ddagger$ ) and the  $\Delta G_{\text{int}}$  to the oxonium intermediate (**5-I**). We were quickly able to discern some trends. While the substitution pattern of the ethereal alkyl group has a notable effect, its overall chain length is irrelevant (compare  $\Delta G^\ddagger$  for Table 3, entries 1 and 2). Steric congestion on the oxygen systematically increases the  $\Delta G^\ddagger$  but lowers the overall  $\Delta G_{\text{int}}$ , thus simply having an effect on reaction rate but not reaction success (compare entries 1–4).

The exception is when both the  $\Delta G^\ddagger$  and the  $\Delta G_{\text{int}}$  are unfavorable (entry 5, Table 3). This explains the observed limited oxidation of phenyl ethers when performing oxidations mediated by **1a**.<sup>20</sup> Similarly, electronic changes have a noticeable effect on both  $\Delta G^\ddagger$  and  $\Delta G_{\text{int}}$ . As may be expected, EDGs lowered  $\Delta G^\ddagger$ , whereas EWGs had the opposite effect. However, the trends in  $\Delta G_{\text{int}}$  are more revealing. Despite having a lower  $\Delta G^\ddagger$  than **5d**, oxidation of **5h** is highly unfavorable, thus explaining the disparity in observed experimental reaction success in these two cases.<sup>19</sup> Additionally, the trends between ethers resulting in ketones (Table 3, entries 9 and 10) follow observed experimental trends in which **5i** succeeded while **5j** failed. This further evidences the idea that the crux of this reaction is the overall  $\Delta G_{\text{int}}$  to **5-I**.

Intrigued by our findings with benzyl ethers, we next examined whether allyl ethers could be oxidized. Initially, we examined the theoretical oxidation of **7d** to its oxonium ion (**7d-I**, Figure 8), without the formation of a dipole-stabilized complex. We were

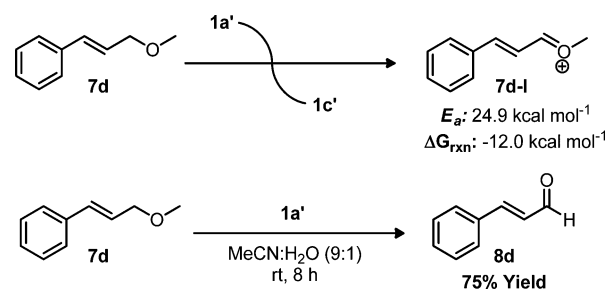


Figure 8. Computational and experimental study on the oxidation of **7d**.

surprised to find that the oxidation not only was favorable from the standpoint of  $\Delta G_{\text{int}}$  but also had a lower  $\Delta G^\ddagger$  than the oxidation of **5a**. These differences may be a consequence of the disparate steric environments between the two substrates and the extended conjugation in the cinnamyl compound. To use this result in a predictive manner, we prepared this compound and subjected it to oxidative cleavage using literature conditions for the cleavage of benzyl ethers. We were pleased to find that this compound could be oxidatively cleaved in good yield (Figure 8).

To test the validity of this hydride transfer model further, we next explored two disparately different substrates: an allylic ester, **7h**, and a nonconjugated allylic ether, **7c**. While both had higher values for  $\Delta G^\ddagger$ , only the acetyl ester had an unfavorable  $\Delta G_{\text{int}}$  to the oxonium intermediate, much like the phenyl ether **5e**. Attempts to oxidize this ester experimentally failed, while oxidation of the nonconjugated allyl ether **7c** succeeded, albeit needing an extended reaction time (Figure 9).

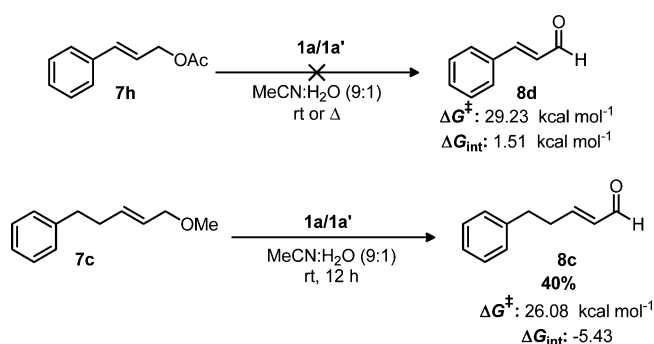
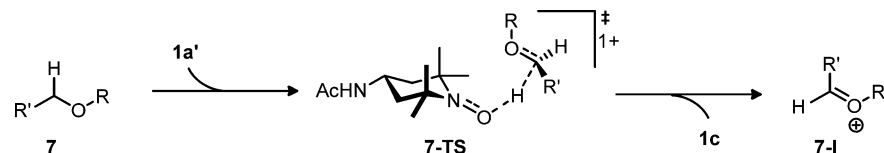


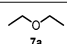
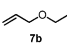
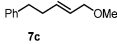
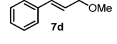
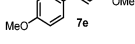
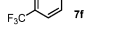
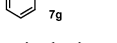
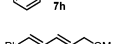
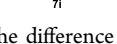
Figure 9. Computational and experimental study on the oxidation of **7h** and **7c**.

On the basis of these encouraging results, we next modeled a series of allyl and nonallyl ethers to extract the factors governing ether oxidation (Table 4). As a reference point, we chose **7d** as it represents a middle ground between extensive alkene stabilization and a complete lack of stabilization. Several trends, which correlate with the benzyl ether counterparts, quickly became apparent. Lack of any olefinic stabilization dramatically increases both  $\Delta G^\ddagger$  and  $\Delta G_{\text{int}}$ , suggesting that oxidation of aliphatic ethers should fail (Table 4, entry 1). The inability of these compounds to undergo oxidation has been confirmed by us and others experimentally.<sup>4,19</sup> Not surprisingly, increasing the substitution pattern and/or extending the conjugation both lowers  $\Delta G^\ddagger$  and stabilizes the intermediate oxonium ion, thus making the process less reversible (compare entries 2 and 3). When the alkene is conjugated, changes to the overall electronics of the  $\pi$  system (even at remote locations within the conjugated system) significantly impacts  $\Delta G^\ddagger$  and  $\Delta G_{\text{int}}$  (entries 5 and 6). Given the results in Table 4, we concluded that a broad range of allyl ethers could likely be oxidized. We pursued this reaction and developed it into a general methodology, which we recently disclosed.<sup>21</sup>

**2.1.3. Oxidative Functionalization of Isochromane.** In 2010, Richter and Garcia-Mancheño disclosed that  $C(\text{sp}^3)\text{-H}$  bonds adjacent to a heteroatom could be functionalized under mild conditions in the presence of stoichiometric amounts of  $\text{TEMP}=\text{O}^+ \text{BF}_4^-$ , **2a** (Figure 10).<sup>22</sup> This dehydrogenative functionalization reaction employs a metal catalyst,  $\text{Fe}(\text{OTf})_2$ , and an enolizable species to accomplish alkylation of the intermediate oxonium ion.

Table 4. Energetics of Allyl and Aliphatic Ether Cleavage Facilitated by 1a'



Entry	Ether	$\Delta G^\ddagger$ (7 to 7-TS) <sup>a</sup>	$\Delta\Delta G^\ddagger_{a,b}$	$\Delta G_{\text{int}}$ (7 to 7-I) <sup>a</sup>	$\Delta\Delta G_{\text{int}}^{a,c}$
1		30.3	4.2	0.6	6.0
2		28.2	2.1	-4.3	1.1
3		26.1	0.0	-5.4	0.0
4		24.9	-1.2	-12.0	-6.6
5		22.2	-3.9	-15.4	-10
6		27.1	1.0	-6.3	-0.9
7		26.3	0.2	-6.1	-0.7
8		29.2	3.1	1.5	6.9
9		21.0	-5.1	-15.1	-9.7

<sup>a</sup>Values in kcal mol<sup>-1</sup>. <sup>b</sup>Defined as the difference in  $\Delta G^\ddagger$  between the current entry and entry 3. <sup>c</sup>Defined as the difference in  $\Delta G_{\text{int}}$  between the current entry and entry 3.

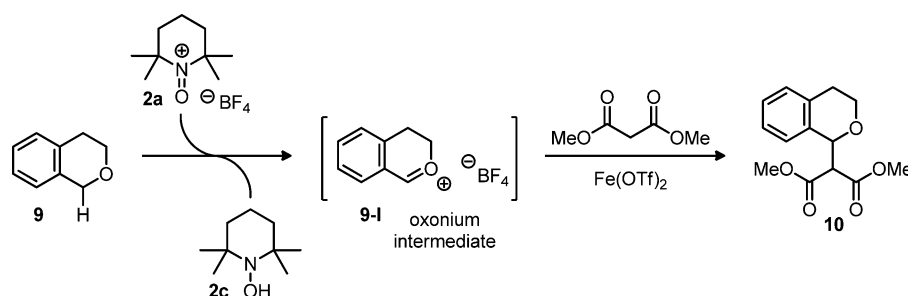


Figure 10. Oxidative functionalization of isochromane mediated by 2a reported by Richter and Garcia-Mancheño.<sup>22</sup>

The key step in the reaction sequence is the formation of the oxonium intermediate (9-I). The authors proposed two putative pathways to this species, one radical and one ionic. Their mechanistic studies were inconclusive, and therefore, the operative mechanism remains in question. To continue our study of oxidations at alkyl groups  $\alpha$  to oxygen, we explored the theoretical oxidative functionalization of isochromane with a diester. The energetics of both the radical and the ionic pathways were calculated, and the respective potential energy surfaces are shown in Figure 11. In the radical pathway, a high-energy single electron transfer (SET) precedes a low barrier hydrogen atom transfer (9'-TS1, red line) while the ionic pathway involves a hydride transfer (9-TS1, green line) in the transition-state structure. The latter was found to be favored by 8.5 kcal mol<sup>-1</sup> compared to the radical pathway. Thus, the likely pathway is ionic.

The formation of the cyclic ether cationic intermediate (9-I) is favorable by -7.0 kcal mol<sup>-1</sup>. This oxonium intermediate then reacts with an iron-enolate complex and has a reasonable activation barrier of 20.7 kcal mol<sup>-1</sup> from the ion and an overall favorable  $\Delta G_{\text{rxn}}$ . The alkylation transition-state structure was

simplified by assuming complete dissociation of the triflate ligands from Fe(OTf)<sub>2</sub>. Multiple conformations of the transition-state structure were computed, with the most energetically favorable structure being that shown in Figure 11. The overall reaction scheme is exergonic, and the theoretical results are in agreement with a reaction that readily proceeds at room temperature.

**2.2. Oxidations  $\alpha$  to Nitrogen.** 2.2.1. *Oxidation of Imines and Amines.* The oxidation of amines to nitriles using 1a has recently been reported by Bailey and co-workers.<sup>18</sup> The reaction is thought to proceed through an imine intermediate which forms following a hydride transfer and a deprotonation. Subsequently, this imine is rapidly oxidized to the nitrile by a second hydride transfer event with a concerted deprotonation. Using ethylamine (11) as a model substrate, the energetics of oxidation were explored computationally in the context of a hydride transfer model, and the results supported their putative mechanism. This sequence is shown in Figure 12. The activation barriers for each hydride transfer event were reasonable (15.8 kcal mol<sup>-1</sup>). Not surprisingly, the activation barrier for a hydride transfer in aliphatic  $\alpha$ -nitrogen substituted cases is markedly



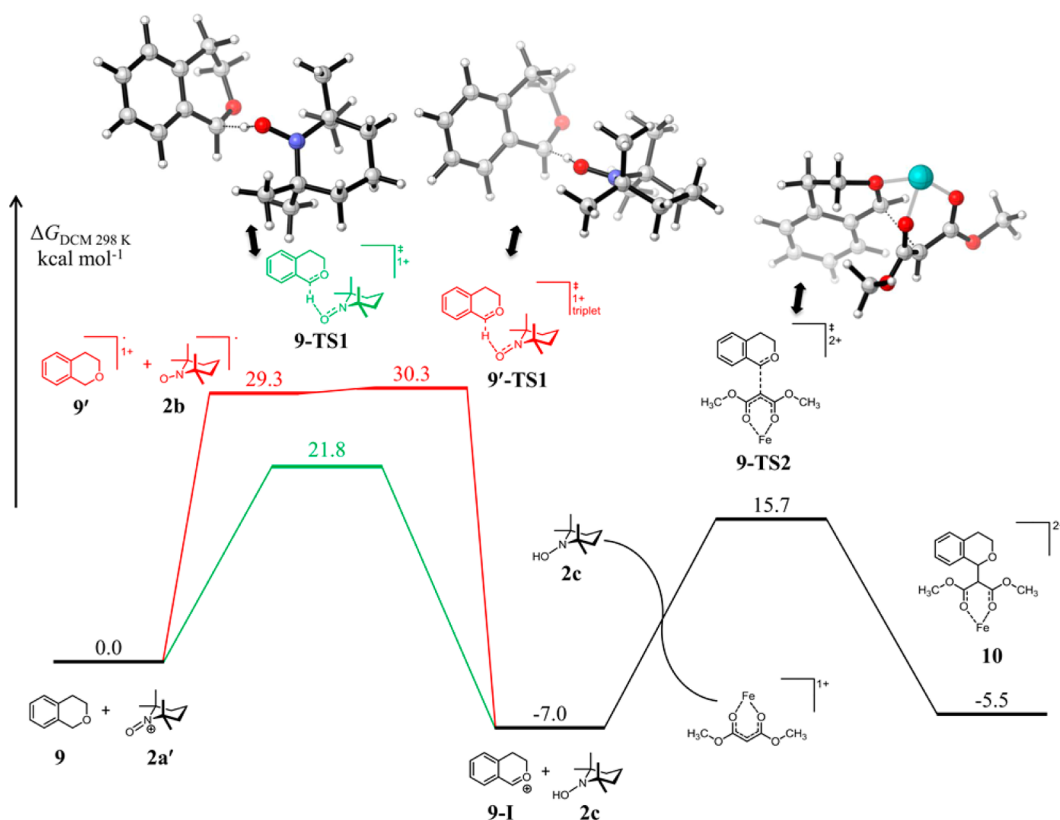


Figure 11. Computed energetic profile for the SET pathway and ionic pathway for the oxidative functionalization of 9.

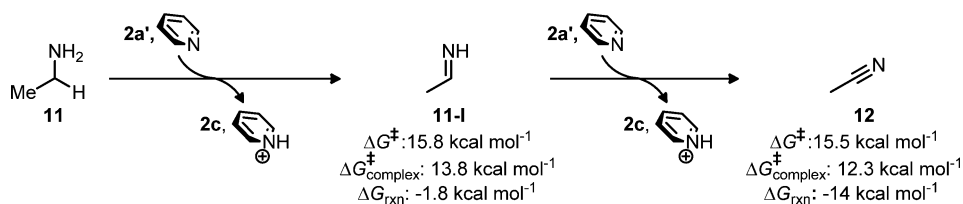


Figure 12. Theoretical oxidation of ethylamine to acetonitrile reported by Bailey and co-workers.<sup>18</sup>

lower than that in analogous  $\alpha$ -oxygen examples, thus supporting the concept that the hydride transfer process is a function of the stability of the forming cationic species. The oxidation to the imine differed in its  $\Delta G_{\text{rxn}}$  as compared to similar oxidations of alcohols to aldehydes ( $\Delta G_{\text{imine}}^{\ddagger}$ :  $-1.8 \text{ kcal mol}^{-1}$  vs  $\Delta G_{\text{aldehyde}}^{\ddagger}$ :  $\approx -20 \text{ kcal mol}^{-1}$ ), but this is to be expected given the disparity in bond strength between  $\text{C}=\text{N}$  and  $\text{C}=\text{O}$  bonds.

We also recently reported on a method to convert aldehydes and alcohols to nitriles using hexamethyldisilazane (HMDS) and **1a**.<sup>23</sup> Mechanistic studies confirmed the intermediacy of an *N*-silyl imine (**13**). Interestingly, this reaction was highly exothermic but required at least room-temperature conditions to initiate. The reaction proceeded rapidly once initiated and resulted in the formation of  $\text{Me}_3\text{Si-F}$  as a byproduct of oxidation. While confident that this oxidation proceeded similarly by a hydride transfer mechanism, we wanted to contrast the energetics of this oxidation with that report by Bailey and co-workers.<sup>18</sup>

The results can be seen in Figure 13. In comparison to the analogous oxidation from an imine to a nitrilium ion, the activation barrier for our more sterically congested *N*-silyl imine is higher ( $>5 \text{ kcal mol}^{-1}$ ). However, the overall  $\Delta G_{\text{rxn}}$  of the process (including desilylation of the intermediate nitrilium ion

with the fluoride anion) is 2.4 times more exergonic ( $-14 \text{ kcal mol}^{-1}$  reported by Bailey and Wiberg vs  $\approx -34 \text{ kcal mol}^{-1}$  reported here). The observed energetic disparities between the two reactions account for the experimental observations.

**2.2.2. Amine Oxidation and Functionalization.** In addition to exploring oxidative functionalization at the  $\alpha$  position to oxygen, Richter and Garcia-Mancheño have also reported that  $\text{C}(\text{sp}^3)\text{-H}$  bonds  $\alpha$  to a nitrogen atom can also be functionalized under mild conditions in the presence of stoichiometric amounts of **2a** and an iron catalyst (Figure 14).<sup>22</sup>

We explored the theoretical oxidation and functionalization of 1,2,3,4-tetrahydroisoquinoline (**15a**) using **2a'** (Figure 15). As in the case of isochromane (**9**), both the radical and the ionic pathways were analyzed (Figure 15). The SET preceding the hydrogen atom transfer was slightly more preferable ( $0.7 \text{ kcal mol}^{-1}$ ) than an ionic hydride transfer. However, taken together with the hydrogen atom transfer step (**15a'-TS1**), the hydride transfer pathway (**15a-TS1**) is kinetically more favorable. Ultimately, both pathways are exergonic and lead to the cyclic iminium ion intermediate (**15a-I**). The activation for the hydride transfer step for this amine substrate is lower than its ether counterpart by  $9.9 \text{ kcal mol}^{-1}$ . This is expected given that nitrogen species are much more easily oxidized by **2a'** than the

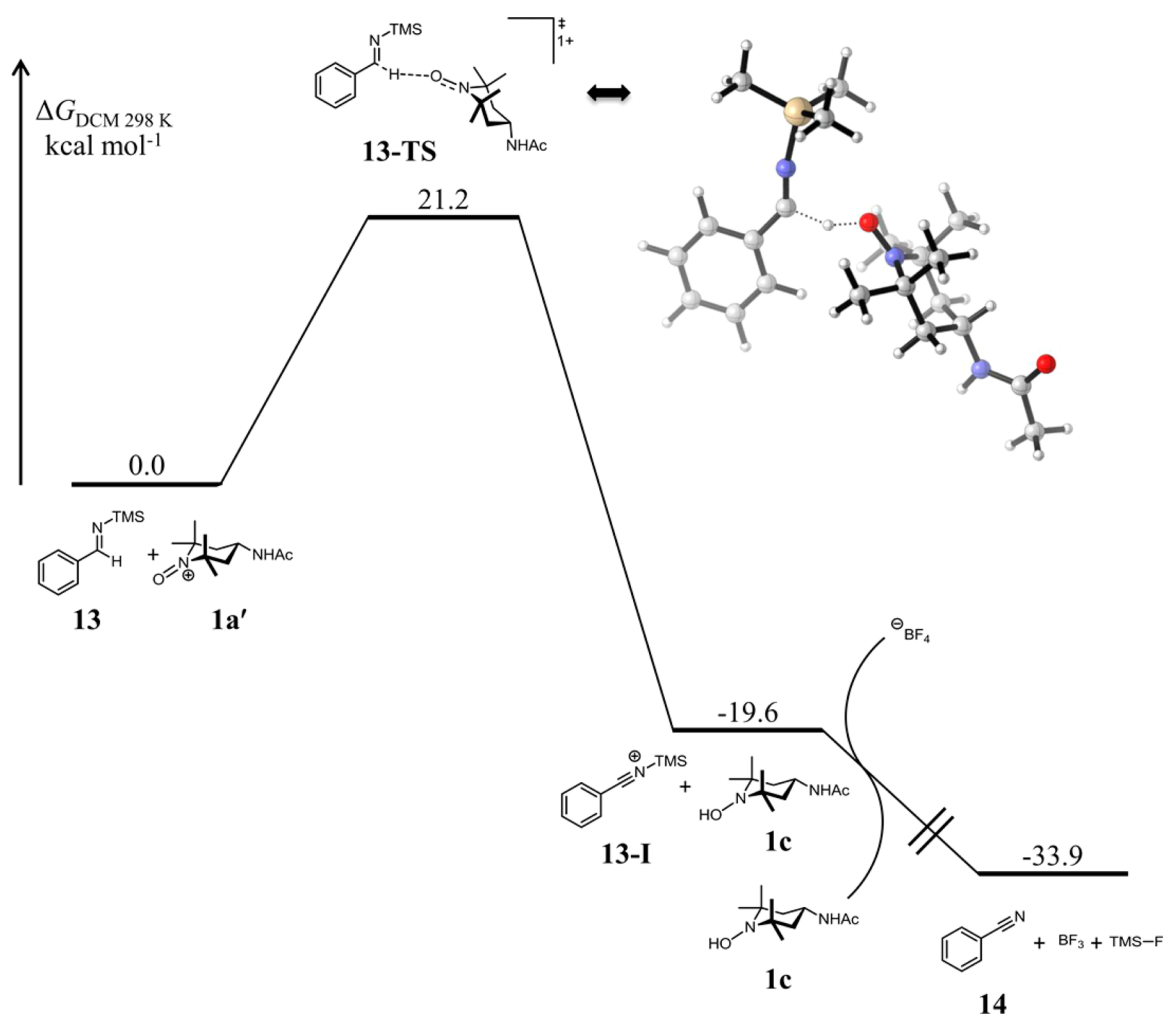


Figure 13. Computed reaction profile for the oxidation of *N*-silyl imines to nitriles.

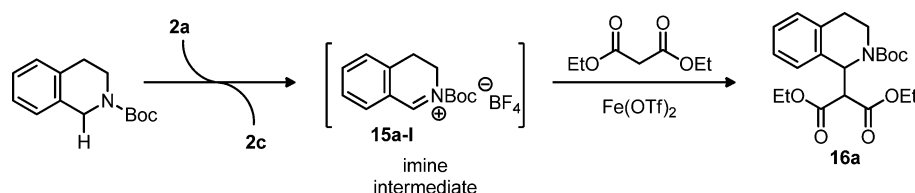


Figure 14. Oxidative functionalization of 1,2,3,4-tetrahydroisoquinolines using **2a** reported by Richter and Garcia-Mancheño.<sup>22</sup>

oxygen containing analogues, likely due to enhanced ability of the nitrogen lone pair to participate in the hydride transfer event. This also matches the observed trend when comparing alcohol and amine oxidations. The reaction leading to the amine intermediate is very energetically favorable and seems to form a cation sink. The reaction of the iminium ion (**15a-I**) with the iron–enolate complex has a relatively high activation barrier of  $31.4 \text{ kcal mol}^{-1}$  (**15a-TS2**) from this energy well. The alkylation of dimethyl malonate is endergonic by  $8.7 \text{ kcal mol}^{-1}$  relative to the iminium ion (which is likely an artifact of the coordination to the iron), but overall exergonic from the starting material.

Unlike isochromane, we can directly influence the electronic nature of the heteroatom in tetrahydroisoquinoline by functionalizing it. We elected to explore one of the substrates experimentally employed by Richter and Garcia-Mancheño, namely, an *N*-acetyl-protected 1,2,3,4-tetrahydroisoquinoline (**15b**).<sup>22</sup> Using this scaffold, we probed the changes in the

energetics of oxidation. When conjugated into the amide functionality, we see a larger disparity between radical (**15b'-TS1**) and ionic pathways (**15b-TS1**). In fact, in this case, the ionic pathway is not only very clearly favored by  $7.7 \text{ kcal mol}^{-1}$  when combining the SET and hydrogen atom steps but also preferred over just the SET step alone by  $3.1 \text{ kcal mol}^{-1}$ . An additional rationale for the overall endergonic nature of this particular reactant is needed. We suggest that, unlike its nonacetylated counterpart, (and the isochromane discussed earlier), it has enhanced steric constraints in its coordinated state. This strain would be relieved upon decomplexation. This lower energy state would prevent the intermediate cation from becoming a thermodynamic sink. Additionally, the irreversibility of forming this C–C bond likely drives this process.

**2.3. Oxidations of Activated C–H Bonds. 2.3.1. Oxidation of Cycloheptatriene.** Cycloheptatriene, **17**, contains a methylene group that is particularly reactive toward oxidation

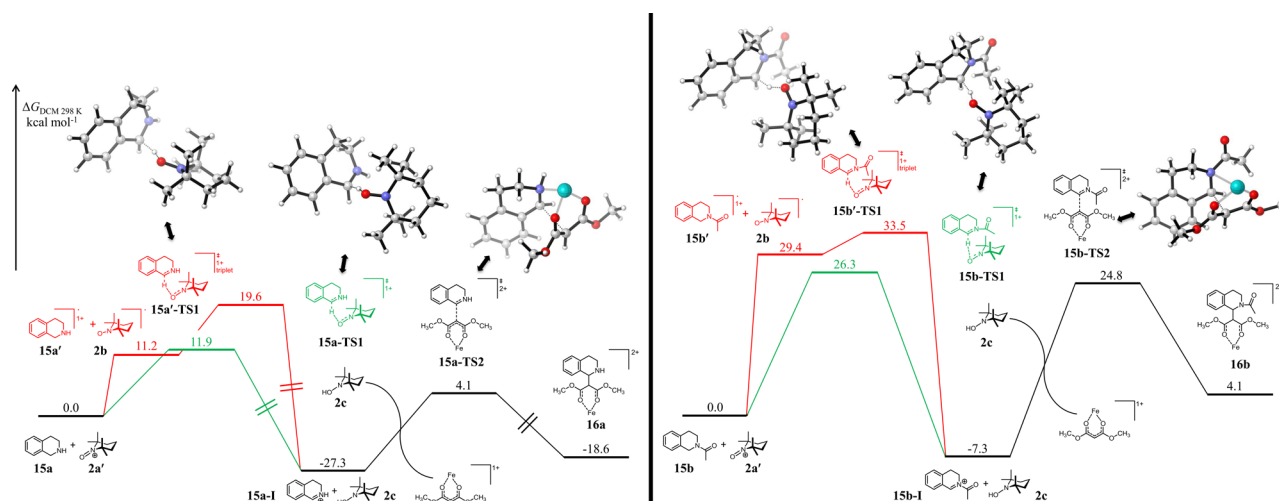


**Figure 15.** Computed reaction profiles for the theoretical oxidative functionalization of 1,2,3,4-tetrahydroisoquinoline (**15a**, left) and its acylated congener (**15b**, right) mediated by **2a'**.

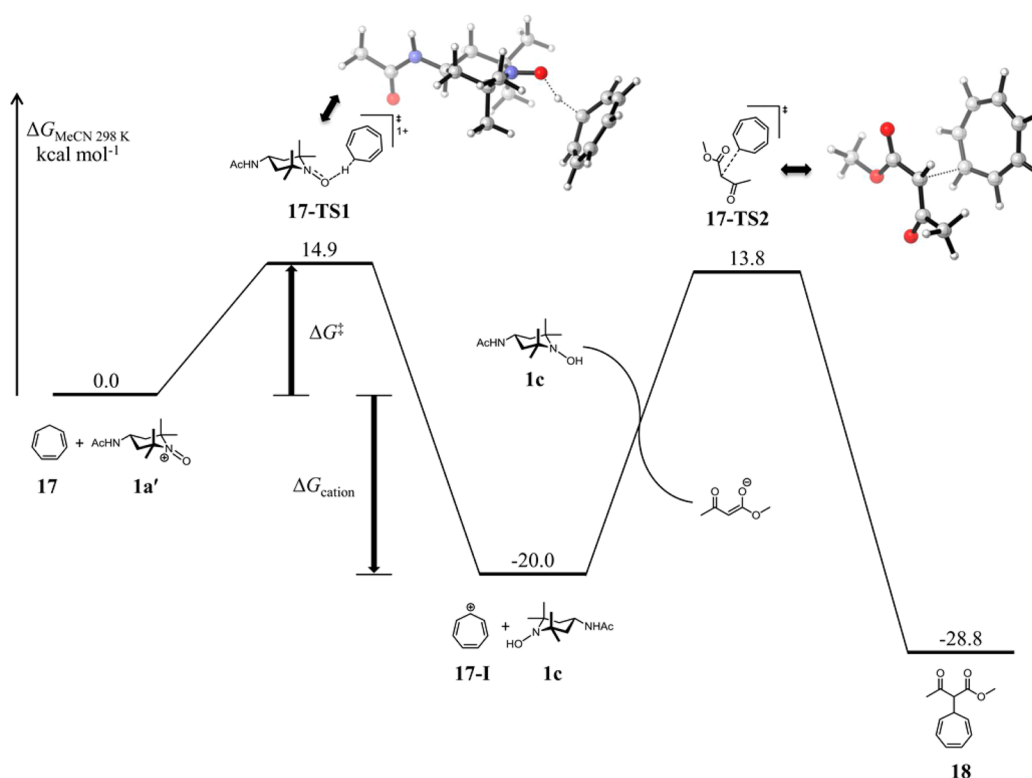


**Figure 16.** Energetics of the theoretical oxidative functionalization of cycloheptatriene mediated by **1a'**.

due to the aromatic tropylium ion that results upon hydride abstraction.<sup>24</sup> This ion can itself be used as an oxidant of certain species such as amines.<sup>25</sup> Given the dual role of the tropylium ion (**17-I**) as both a hydride acceptor (an oxidizing agent remarkably similar to the oxoammonium cation) and a hydride donor, some ambiguity exists as to whether an oxidation of **17** by an oxoammonium salt would be possible. Electrochemical studies using **2b** suggested that it may be plausible using **1a**.<sup>26</sup> We modeled the oxidation involving a putative hydride transfer event (Figure 16, **17-TS1**) using the parameters for acetonitrile in our solvation model. The  $\Delta G^\ddagger$  for the hydride transfer was quite modest, and the  $\Delta G_{\text{cation}}$  was highly favorable. We next modeled an alkylation reaction (**17-TS2**) with the free enolate of methyl

acetoacetate. The activation barrier for this event was rather high from the tropylium ion (likely due to dearomatization), but the overall reaction was exergonic. On the basis of this potential energy surface, we speculated that oxidative functionalization of **17** should proceed readily. We, therefore, attempted this net process experimentally. Oxidation did indeed proceed rapidly and was complete in less than 1 h, as confirmed by the presence of the characteristic  $^1\text{H}$  NMR signal of the tropylium cation at 9.36 ppm. Unfortunately, attempts to isolate tropylium tetrafluoroborate proved problematic due to the near identical solubility properties of **1c** and this tropylium salt. Rather than isolate the ion, we proceeded to functionalize it in a manner similar to our theoretical oxidation. Conrow reported that

tropylium tetrafluoroborate can be effectively functionalized in the presence of acetylacetone and pyridine.<sup>27</sup> Using this report and our computations as a guide, we conducted the sequence outlined in Figure 18. After a short optimization of workup conditions based on the relative solubilities of **1c** and **18**, we were able to isolate the functionalized cycloheptatriene in good yield (Figure 17). This experimental result is the strongest support to date for the hydride transfer model in oxoammonium salt oxidations to date.

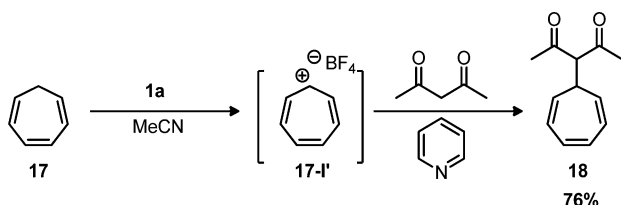


**Figure 17.** Experimental oxidative functionalization of **17** mediated by **1a**.

**2.3.2. Allylic Oxidation.** On the basis of the results with **17**, we wondered whether the reported facile reaction of an oxoammonium species with a trisubstituted alkene reported<sup>28</sup> by Bailey and co-workers also proceeded by a hydride transfer pathway. The reaction leads to the formation of allylic alkoxyamines (Figure 18). Bailey suggested that this reaction

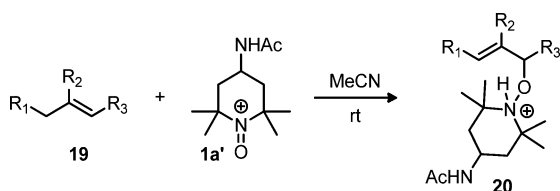


**Figure 18.** Ene-like addition of the **1a'** to alkenes.

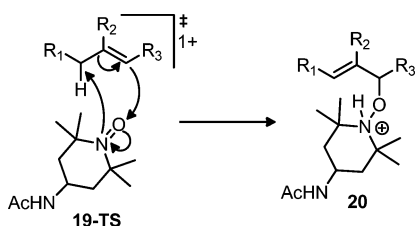


**Figure 19.** Ene-like mechanism proposed by Bailey and co-workers<sup>28</sup> leading to allylic alkoxyamines.

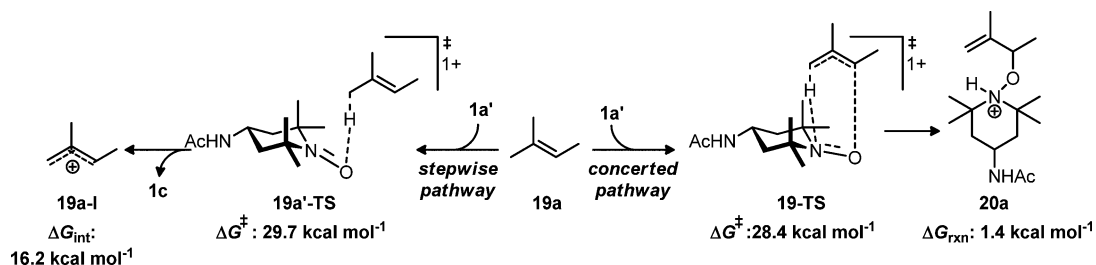


**Figure 20.** Ene-like mechanism proposed by Bailey and co-workers<sup>28</sup> leading to allylic alkoxyamines.

proceeds through a concerted ene-like mechanism (Figure 19).<sup>27</sup> The nucleophilic addition was said to occur in a simultaneous manner with removal of the allylic proton and C–O bond formation. To determine the operative pathway, we explored the energetics of both the literature proposed route as well as our putative hydride transfer mechanism. When modeling the former (Figure 20), we found the process to be concerted as previously posited. The activation barrier for the ene-like process (**19-TS**) was found to be 28.4 kcal mol<sup>-1</sup> for 2-methyl-2-butene as a substrate. Comparatively, the rate-determining hydride transfer step in the theoretical stepwise pathway (**19-TS'**) has an activation barrier of 29.7 kcal mol<sup>-1</sup>. The  $\Delta\Delta G^\ddagger$  between the hydride transfer and the ene-like pathway is modest (1.3 kcal mol<sup>-1</sup>). Each respective transition-state structure is shown in Figure 21. Unlike the oxidation of the tropylium ion, the  $\Delta G_{\text{cation}}$  is highly unfavorable when proceeding via the stepwise pathway. Thus, the resulting cation is a stronger oxidant (i.e., a better hydride acceptor) than the oxoammonium cation. Therefore, just as in the oxidation of benzyl ethers, a thermodynamically unfavorable hydride transfer results in the inability to proceed forward in the reaction, and although kinetically equal, the unfavorable  $\Delta G_{\text{int}}$  precludes a hydride transfer mechanism in this reaction.

**2.3.3. Oxidation of Other Activated C–H Bonds.** Given the results on the theoretical oxidation of reactive C–H bonds in the preceding sections, we became interested in the factors influencing oxidation of C–H bonds using the putative hydride transfer model. We, therefore, modeled a range of compounds possessing such C–H bonds with various steric and electronic environments. The computed results are in Table 5.

In general, the determining factor for oxidation of such bonds by **1a'** is not kinetic in origin but thermodynamic, supporting our earlier assertions in the case of the oxidation of allyl and benzyl ethers. Oxidations leading to cyclopropenium ions (Table 5, entries 1–5) are highly favorable kinetically and thermodynamically, though not to the same degree as **17**. Electronic changes do have an effect on both energetic parameters with a magnitude similar to those of allyl and benzyl ethers. For example, the electron-donating *p*-OMe group (entry 2) both stabilizes the corresponding cyclopropenium ion thermodynamically and lowers  $\Delta G^\ddagger$ , making the hydride transfer more preferable kinetically. Steric effects in this case are only noticeable when adding groups at the incipient cationic center (compare  $\Delta G^\ddagger$  of entries 1, 4, and 5). Oxidations resulting in stabilized, but nonaromatic, ions face steeper challenges. Unless highly stabilized, such as in the case of the trityl group (entry 6), oxidation is an endergonic process. Thus, oxidation in these systems is likely to be difficult, if not impossible. Indeed, to date, we have not observed oxidation experimentally for toluene, diphenylmethane, or norbornadiene (entries 7, 8, and 9). Similarly, oxidation of triphenylmethane has not met with

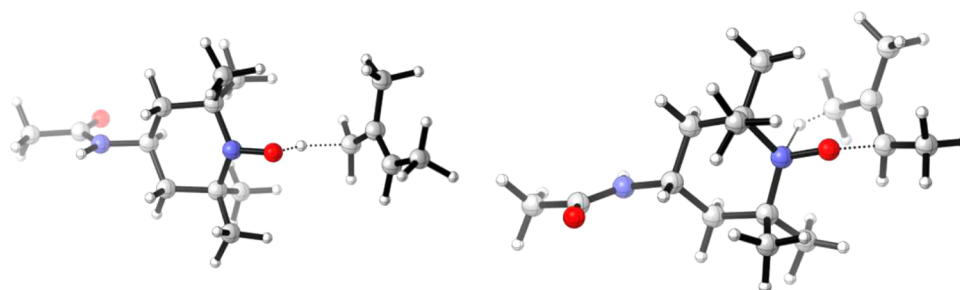


Figure 21. Transition-state structures for the ene-like reaction, stepwise hydride transfer TS (left, 19a-TS), concerted cyclic TS (right, 19a'-TS).

Table 5. Energetics of the Theoretical Oxidation of Activated C–H Bonds<sup>a</sup>

Entry	C-H Bond	$\Delta G^{\ddagger a}$ (21 to 21-TS)	$\Delta G_{\text{cation}}^a$ (21 to 21-I)
1		19.9	-10.2
2		17.6	-14.0
3		22.5	-6.7
4		17.0	-13.9
5		21.4	-20.4
6		34.5	-1.9
7		30.9	7.6
8		35.7	23.2
9		37.0	7.4

<sup>a</sup>All values are in kcal mol<sup>-1</sup>.

experimental success by us to date. This latter observation likely relates to the high value of  $\Delta G^{\ddagger}$  for oxidation rather than the thermodynamics of the reaction. A high activation barrier in this case is likely a consequence of the sterically hindered environment surrounding the C–H bond and the need to form a planar geometry upon carbocation formation. In fact, the failure of this oxidation is the exact evidence used by Semmelhack et al. to discount a hydride transfer mechanism for oxidations involving oxoammonium cations. However, the hydride transfer model we suggest explains both the failure of triphenylmethane and the success of cycloheptatriene to oxidize.<sup>29</sup>

### 3. CONCLUSION

In closing, we have thoroughly explored the validity of a hydride transfer mechanism for oxoammonium cations in an array of different oxidative reactions. A hydride transfer-based model appears to be a viable mechanistic path for oxidations at positions  $\alpha$  to oxygen and nitrogen as well as in activated (prearomatic) compounds. This hydride transfer model explains experimental trends and can be used to predict reactivity during oxidations. Electronic influences by groups neighboring the hydridic hydrogen as well as steric constraints given the bulky nature of the 2,2,6,6-tetramethylpiperidyl scaffold have significant con-

tributions to the energetics (and ultimately the reactivity) in oxidations. Several reactions discussed here, specifically the oxidation of cycloheptatriene, lend credence to a hydride transfer mechanism being operative. Such a finding supports the notion that the hydride transfer mechanism originally discounted by Semmelhack et al. is a valid alternative to the currently accepted mechanism for oxoammonium cation-mediated oxidations.

### 4. EXPERIMENTAL SECTION

**General Considerations.** All chemical transformations requiring inert atmospheric conditions or vacuum distillation utilized Schlenk line techniques with a 3- or 4-port dual-bank manifold. Nitrogen was used to provide such an atmosphere. NMR spectra (<sup>1</sup>H, <sup>13</sup>C, <sup>19</sup>F) were performed at 298 K on either a 300, 400, or 500 MHz NMR. <sup>1</sup>H NMR spectra obtained in CDCl<sub>3</sub> were referenced to residual nondeuterated chloroform (7.26 ppm) in the deuterated solvent. <sup>13</sup>C NMR spectra obtained in CDCl<sub>3</sub> were referenced to CDCl<sub>3</sub> (77.3 ppm). <sup>19</sup>F NMR spectra were referenced to hexafluorobenzene (–164.9 ppm).<sup>30</sup> IR spectra were obtained on an FT-IR spectrometer. Reactions were monitored by a gas chromatograph attached to a mass spectrometer, <sup>1</sup>H NMR, and/or by TLC on silica gel plates (60 Å porosity, 250 μm thickness). TLC analysis was performed using hexanes/ethyl acetate as the eluent and visualized using permanganate stain, *p*-anisaldehyde stain, Seebach's Stain, and/or UV light. Flash chromatography and silica plugs

utilized Dynamic Adsorbents Inc. Flash Silica Gel (60 Å porosity, 32–63  $\mu\text{m}$ ).

**Chemicals.**  $\text{CDCl}_3$  was stored over 4 Å molecular sieves. Alcohols used for relative rate studies were purchased from commercial suppliers. The oxoammonium salt 4-acetamido-2,2,6,6-tetramethyl-1-oxopiperidin-1-ium tetrafluoroborate, **1a**, was prepared according to our recently published protocol.<sup>4b</sup>

**Synthesis of  $\alpha$ -Fluoro and  $\alpha$ -Difluoro Carbinols via Their Respective Ketones.** *1-Fluoro-4-phenylbutan-2-one*<sup>37</sup> (**4n**). The following is a modification of the procedure outlined by Alexakis and co-workers.<sup>31</sup> To a 50 mL round-bottom flask were added crushed magnesium turnings (1.23 g, 50.4 mmol, 1.44 equiv) and a stir bar. The flask was sealed with a rubber septum, the atmosphere was evacuated from the flask via an inlet needle, and the flask was flame-dried under vacuum. The flask was cooled by flushing with nitrogen and then placed in a room-temperature water bath. (2-Bromoethyl)benzene (7.77 g, 42 mmol, 1.2 equiv) was dissolved in a minimal amount of anhydrous  $\text{Et}_2\text{O}$  (16 mL) and added dropwise to the flask. **Caution!** Exothermic. After complete addition, the solution was allowed to stir at room temperature for 1 h and the mixture gradually became dark gray.

In a separate flame-dried 500 mL round-bottom flask equipped with a stir bar, rubber septum, and  $\text{N}_2$  inlet needle were added fluoroacetonitrile (2.07 g, 35 mmol, 1 equiv) and anhydrous  $\text{Et}_2\text{O}$  (210 mL, 0.166 M in the nitrile). The flask was cooled to 0 °C via an ice–water bath and stirred at this temperature for 5 min. After this time, the Grignard solution was transferred to a syringe and added to this chilled flask over the course of 15 min. The solution was allowed to stir at 0 °C for 2 h, whereupon a white precipitate formed. After this time, the solution was quenched with saturated 10% aqueous HCl. The biphasic mixture was transferred to a separatory funnel and diluted with  $\text{Et}_2\text{O}$  (100 mL) and deionized water (100 mL). The phases were separated, and the aqueous layer was extracted with  $\text{Et}_2\text{O}$  (3  $\times$  100 mL). The combined organic layers were washed with deionized water ( $\approx$ 200 mL) and brine ( $\approx$ 200 mL) and dried with  $\text{Na}_2\text{SO}_4$ . The solvent was removed *in vacuo* by rotary evaporation. The crude ketone was purified by vacuum distillation (53–55 °C @ 0.1 mmHg) to give the pure  $\text{CFH}_2$  ketone (4.18 g, 72%) as a clear, colorless oil. <sup>1</sup>H NMR ( $\text{CDCl}_3$ , 400 MHz)  $\delta$  ppm 2.87–2.94 (m, 2 H) 2.99 (apparent triplet,  $J = 7.70$  Hz, 2 H) 4.79 (d,  $J = 47.59$  Hz, 1 H) 7.25 (apparent triplet,  $J = 7.50$  Hz, 3 H) 7.33 (apparent triplet  $J = 7.30$  Hz, 2 H); <sup>13</sup>C NMR ( $\text{CDCl}_3$ , 100 MHz)  $\delta$  ppm 28.9 (d,  $J_{\text{C-C-C-F}} = 1.8$  Hz,  $\text{CH}_2$ ) 40.1 ( $\text{CH}_2$ ) 85.3 (d,  $J_{\text{C-F}} = 184.9$  Hz,  $\text{CH}_2$ ) 126.6 (CH) 128.55 (CH) 128.8 (CH) 140.7 (C) 206.3 (d,  $J_{\text{C-C-F}} = 19.4$  Hz, C); <sup>19</sup>F NMR ( $\text{CDCl}_3$ , 377 MHz)  $\delta$  ppm –230.79 (t,  $J = 47.70$  Hz); GC–MS (EI) 166 ( $[\text{M}]^+$ , 43%) 133 (44%) 115 (8%) 105 (82%) 91 (100%) 77 (28%) 65 (16%) 61 (6%) 51 (14%).

*1-Fluoro-4-phenylbutan-2-ol*<sup>32</sup> (**3n**). To a 100 mL round-bottom flask equipped with a stir bar was added the  $\alpha$ -fluoro ketone **4n** (3.18 g, 0.0191 mol) dissolved in methanol (40 mL). The flask was cooled to 0 °C via an ice–water bath. After stirring at 0 °C for 10 min,  $\text{NaBH}_4$  (1.46 g, 0.0386 mol, 2 equiv) was added slowly portionwise to the flask. **Caution!** Exothermic, evolves  $\text{H}_2$  gas. The reaction mixture was allowed to stir at 0 °C for 5 min after complete addition of  $\text{NaBH}_4$ . The flask was then warmed to room temperature and allowed to stir for 2 h. After this time, the reaction was carefully quenched with deionized  $\text{H}_2\text{O}$  (30 mL). The quenched reaction mixture was transferred to a separatory funnel and diluted with deionized water (100 mL) and  $\text{Et}_2\text{O}$  (150 mL). The layers were separated, and the aqueous layer was extracted with  $\text{Et}_2\text{O}$  (3  $\times$  75 mL). The combined organic layers were washed with deionized  $\text{H}_2\text{O}$  (2  $\times$  100 mL) and brine (150 mL). The organic layer was dried with  $\text{Na}_2\text{SO}_4$ , and the solvent was removed *in vacuo* by rotary evaporation to give the crude alcohol. Further purification was accomplished by vacuum distillation (59–62 °C @ 0.1 mmHg) to give the desired alcohol **3n** (2.46 g, 76%) as a clear, colorless oil. <sup>1</sup>H NMR ( $\text{CDCl}_3$ , 400 MHz)  $\delta$  ppm 2.12–2.31 (m, 2 H) 2.46 (d,  $J = 4.72$  Hz, 1 H) 3.09–3.20 (m, 1 H) 3.22–3.34 (m, 1 H) 4.23–4.39 (m, 1 H) 4.62–4.94 (m, 2 H) 7.59–7.67 (m, 3 H) 7.69–7.75 (m, 2 H); <sup>13</sup>C NMR ( $\text{CDCl}_3$ , 100 MHz)  $\delta$  ppm 31.8 ( $\text{CH}_2$ ) 33.7 (d,  $J_{\text{C-C-F}} = 6.4$  Hz,  $\text{CH}_2$ ) 70.0 (d,  $J_{\text{C-F}} = 18.7$  Hz, CH) 87.2 (d,  $J_{\text{C-F}} = 168.6$  Hz,  $\text{CH}_2\text{F}$ ) 126.3 (CH) 128.7 (CH) 128.8 (CH) 141.6 (C); <sup>19</sup>F NMR ( $\text{CDCl}_3$ , 377 MHz)  $\delta$  ppm –231.55 (td,  $J = 47.29, 18.28$  Hz); GC–MS (EI) 168

( $[\text{M}]^+$ , 8%) 150 (20%) 117 (76%) 115 (16%) 105 (16%) 91 (100%) 77 (23%) 65 (25%) 63 (14%) 51 (13%) 43 (11%) 369 (12%).

*2,2-Difluoro-1-(p-tolyl)ethanone*<sup>33</sup> (**4o**). To a 100 mL round-bottom flask were added crushed magnesium turnings (2.92 g, 0.120 mol, 1.2 equiv) and a stir bar. The flask was sealed with a rubber septum, the atmosphere was evacuated from the flask via an inlet needle, and the flask was flame-dried under vacuum. The flask was flushed with nitrogen and placed in a room-temperature water bath. *p*-Bromotoluene (17.16 g, 0.100 mol, 1 equiv) was dissolved in a minimal amount of anhydrous  $\text{Et}_2\text{O}$  (45 mL) and added dropwise to the flask. **Caution!** Exothermic. After complete addition, the solution was allowed to stir at room temperature for 1 h and the mixture gradually became dark gray.

To a separate flame-dried 250 mL round-bottom flask equipped with a stir bar, rubber septum, and  $\text{N}_2$  inlet needle were added ethyl difluoroacetate (15.63 g, 0.110 mol, 1.1 equiv) and anhydrous  $\text{Et}_2\text{O}$  (61 mL). The flask was cooled to –78 °C via a dry ice/acetone bath and stirred at this temperature for 5 min. After this time, the Grignard solution was transferred to a syringe and added to this chilled flask over 15 min. The solution was allowed to stir at –78 °C for 3 h. After this time, the solution was warmed to room temperature and was quenched with saturated  $\text{NH}_4\text{Cl}$ . The quenched mixture was warmed to 0 °C and a 0.5 M aqueous  $\text{H}_2\text{SO}_4$  solution (75 mL) was added. The biphasic mixture was transferred to a separatory funnel and diluted with pentane (100 mL) and deionized water (100 mL). The phases were separated, and the aqueous layer was extracted with pentane (3  $\times$  50 mL). The combined organic layers were washed with brine and dried with  $\text{Na}_2\text{SO}_4$ . The solvent was removed *in vacuo* by rotary evaporation. The crude ketone was purified by recrystallization (hexanes) to give the pure  $\text{CF}_2\text{H}$  ketone (8.92 g, 52%) as an off-white, crystalline solid (mp 48–50 °C). <sup>1</sup>H NMR ( $\text{CDCl}_3$ , 400 MHz)  $\delta$  ppm 2.45 (s, 3 H) 6.27 (t,  $J = 53.62$  Hz, 1 H) 7.33 (dd,  $J = 8.56, 0.58$  Hz, 2 H) 7.98 (d,  $J = 8.17$  Hz, 2 H); <sup>13</sup>C NMR ( $\text{CDCl}_3$ , 100 MHz)  $\delta$  ppm 22.2 ( $\text{CH}_3$ ) 111.5 (t,  $J_{\text{C-F}} = 253.5$  Hz,  $\text{CF}_2\text{H}$ ) 129.4 (t,  $J_{\text{C-C-F}} = 1.5$  Hz, C) 130.0 (CH) 130.0 (t,  $J_{\text{C-C-C-F}} = 2.3$  Hz, CH) 146.5 (C) 187.5 (t,  $J_{\text{C-C-F}} = 25.4$  Hz, C); <sup>19</sup>F NMR ( $\text{CDCl}_3$ , 377 MHz)  $\delta$  ppm –173.13 (d,  $J = 53.13$  Hz); GC–MS (EI) 170 ( $[\text{M}]^+$ , 4%), 119 (100%), 91 (82%), 89 (14%), 65 (32%), 63 (15%), 51 (17%), 39 (11%).

*2,2-Difluoro-1-(p-tolyl)ethanol*<sup>34</sup> (**3o**). To a 100 mL round-bottom flask equipped with a stir bar was added the  $\alpha$ -difluoro ketone **4o** (4.00 g, 0.0235 mol) dissolved in methanol (47 mL). The flask was cooled to 0 °C via an ice–water bath. After stirring at 0 °C for 10 min,  $\text{NaBH}_4$  (1.79 g, 0.0470 mol, 2 equiv) was added slowly portionwise to the flask. **Caution!** Exothermic, evolves  $\text{H}_2$  gas. The reaction mixture was allowed to stir at 0 °C for 5 min after complete addition of  $\text{NaBH}_4$ . The flask was then warmed to room temperature and allowed to stir for 2 h. After this time, the reaction was carefully quenched with deionized  $\text{H}_2\text{O}$  (30 mL). The quenched reaction mixture was transferred to a separatory funnel and diluted with deionized water (100 mL) and  $\text{Et}_2\text{O}$  (150 mL). The layers were separated, and the aqueous layer was extracted with  $\text{Et}_2\text{O}$  (3  $\times$  75 mL). The combined organic layers were washed with deionized  $\text{H}_2\text{O}$  (2  $\times$  100 mL) and brine (150 mL). The organic layer was dried with  $\text{Na}_2\text{SO}_4$ , and the solvent was removed *in vacuo* by rotary evaporation to give the crude alcohol. Further purification was accomplished by vacuum distillation (56–58 °C @ 0.1 mmHg) to give the desired alcohol **3o** (3.37 g, 83%) as a clear, colorless oil. <sup>1</sup>H NMR ( $\text{CDCl}_3$ , 400 MHz)  $\delta$  ppm 2.38 (s, 3 H) 2.51 (br. s., 1 H) 4.78 (tt,  $J = 10.30, 3.90$  Hz, 1 H) 5.76 (td,  $J = 56.05, 4.77$  Hz, 1 H) 7.22 (d,  $J = 7.98$  Hz, 2 H) 7.31 (d,  $J = 7.69$  Hz, 2 H); <sup>13</sup>C NMR ( $\text{CDCl}_3$ , 100 MHz)  $\delta$  ppm 21.5 ( $\text{CH}_3$ ) 73.8 (t,  $J_{\text{C-F}} = 24$  Hz, CH) 116.2 (t,  $J_{\text{C-F}} = 245.3$  Hz,  $\text{CF}_2\text{H}$ ) 127.3 (CH) 129.7 (CH) 133.2 (t,  $J_{\text{C-C-F}} = 3.4$  Hz, C) 139.2 (C); <sup>19</sup>F NMR ( $\text{CDCl}_3$ , 377 MHz)  $\delta$  ppm –130.43 (dd,  $J = 55.86, 9.53$  Hz); GC–MS (EI) 172 ( $[\text{M}]^+$ , 9%) 121 (81%) 93 (80%) 91 (100%) 77 (65%) 65 (26%) 63 (17%) 51 (56%) 39 (15%).

**Synthesis of Allyl Ethers and Related Substrates.** (*E*)-3-Methoxyprop-1-en-1-ylbenzene (**7d**). The following procedure is a modification of the protocol outlined by Mastsubara and Jamison.<sup>35</sup> To a flame-dried 250 mL round-bottom flask equipped with a stir bar was added  $\text{NaH}$ <sup>36</sup> (2.40 g, 0.100 mol, 2 equiv), followed by anhydrous THF (125 mL). The flask was sealed with a rubber septum and placed under a  $\text{N}_2$  atmosphere via an inlet needle. Cinnamyl alcohol (6.71 g, 0.050 mol,

1 equiv) dissolved in a minimum amount of THF ( $\approx 10$  mL) was added to the flask dropwise over 10 min. **Caution!** Mildly exothermic, evolves  $H_2$  gas. The reaction mixture was allowed to stir at room temperature for 1.5 h, during which time the solution transitioned from a pale yellow to an orangish-red. After this time, MeI (21.30 g, 0.150 mol, 3 equiv) was added to the flask and the solution was allowed to stir for 6 h at room temperature.<sup>37</sup> The reaction mixture was then carefully quenched with deionized water ( $\approx 30$  mL) and transferred to a separatory funnel. The mixture was diluted with deionized water (150 mL) and  $Et_2O$  (150 mL), and the layers were separated. The aqueous layer was extracted with  $Et_2O$  ( $3 \times 75$  mL), and the combined organic layers were washed with deionized water ( $2 \times 100$  mL), followed by brine (150 mL). The organic layer was dried with  $Na_2SO_4$ , and the solvent was removed *in vacuo* by rotary evaporation to give the crude ether. Further purification was accomplished by  $SiO_2$  plug (95:5 to 9:1 Hex:EtOAc) to give the pure ether **7d** (5.74 g, 77%) as a clear, pale yellow oil.  $^1H$  NMR ( $CDCl_3$ , 400 MHz)  $\delta$  ppm 3.45 (s, 3 H) 4.15 (dd,  $J = 5.98, 1.22$  Hz, 2 H) 6.36 (dt,  $J = 15.94, 5.95$  Hz, 1 H) 6.68 (d,  $J = 16.01$  Hz, 1 H) 7.30 (t,  $J = 7.10$  Hz, 1 H) 7.38 (t,  $J = 7.52$  Hz, 2 H) 7.46 (d,  $J = 7.69$  Hz, 2 H);  $^{13}C$  NMR ( $CDCl_3$ , 100 MHz)  $\delta$  ppm 58.0 ( $CH_3$ ), 73.1 ( $CH_2$ ), 126.1 (CH), 126.6 (CH), 127.8 (CH), 128.7 (CH), 132.5 (CH), 136.9 (C); GC-MS (EI) 148 ( $[M]^+$ , 13%) 131 (100%) 115 (30%) 103 (88%) 91 (14%) 77 (81%) 63 (25%) 51 (61%) 39 (17%).

**Cinnamyl Acetate**<sup>38</sup> (**7h**). To a 100 mL round-bottom flask equipped with a stir bar were added cinnamyl alcohol (6.71 g, 0.050 mol, 1 equiv) and  $CH_2Cl_2$  (10 mL). The flask was cooled to  $0^\circ C$  in an ice bath for 10 min. After this time, acetic anhydride (17.1 g, 0.167 mol, 3.4 equiv) was added, followed by dropwise addition of pyridine (13.21 g, 0.167 mol, 3.4 equiv). The solution was allowed to stir for 30 min at  $0^\circ C$ . After this time, the solution was allowed to warm to room temperature and was stirred overnight. The solution was transferred to a separatory funnel and diluted with 150 mL of  $CH_2Cl_2$  and 150 mL of aqueous 2 M HCl. The layers were separated, and the acid layer was extracted with  $CH_2Cl_2$  ( $2 \times 50$  mL). The combined organic layers were washed with 2 M HCl (100 mL), saturated aqueous  $NaHCO_3$  ( $2 \times 100$  mL), deionized  $H_2O$  (100 mL), and brine (150 mL). The organic layer was dried with  $Na_2SO_4$ , and the solvent was removed *in vacuo* by rotary evaporation to give the crude acetate. Further purification was accomplished by vacuum distillation ( $93-95^\circ C$  @ 0.3 mmHg) to give the pure acetate **7h** (7.03 g, 80%) as a clear, colorless oil.  $^1H$  NMR ( $CDCl_3$ , 400 MHz)  $\delta$  ppm 2.12 (s, 3 H) 4.76 (d,  $J = 6.42$  Hz, 2 H) 6.32 (dt,  $J = 15.90, 6.43$  Hz, 1 H) 6.68 (d,  $J = 15.91$  Hz, 1 H) 7.29 (t,  $J = 7.20$  Hz, 1 H) 7.35 (t,  $J = 7.47$  Hz, 2 H) 7.42 (d,  $J = 7.15$  Hz, 2 H);  $^{13}C$  NMR ( $CDCl_3$ , 100 MHz)  $\delta$  ppm 21.1 ( $CH_3$ ) 65.1 ( $CH_2$ ) 123.3 (CH) 126.7 (CH) 128.2 (CH) 128.7 (CH) 134.3 (CH) 136.3 (C) 170.8 (C); GC-MS (EI) 176 ( $[M]^+$ , 14%) 134 (25%) 117 (36%) 116 (38%) 115 (100%) 105 (40%) 103 (21%) 91 (30%) 77 (36%) 63 (13%) 51 (18%) 43 (90%).

**(E)-(5-Methoxypent-3-en-1-yl)benzene (7c) from 3-Phenyl-1-propanol.** **3-Phenylpropanal.**<sup>39</sup> To a 500 mL round-bottom flask equipped with a stir bar, were added 3-phenyl-1-propanol (13.62 g, 0.100 mol, 1 equiv) and  $CH_2Cl_2$  (200 mL). The oxoammonium salt **1a** (4.50 g, 0.015 mol, 0.15 equiv) was added to the solution. While stirring, commercial bleach (8.25% w/w) (90.18 g, 0.100 mol, 1 equiv) was added all at once. The solution turned from a bright yellow to bright red color. The solution was allowed to stir vigorously at room temperature for 2 h and monitored by  $^1H$  NMR to assess reaction completion. The reaction was judged to be complete at this time. The reaction mixture was transferred to a separatory funnel and diluted with 75 mL of deionized water and extracted with  $CH_2Cl_2$  ( $3 \times 75$  mL). The combined organic extractions were washed with 150 mL of deionized water, followed by 150 mL of brine. The organic layer was then dried with  $Na_2SO_4$ . The solvent was removed *in vacuo* by rotary evaporation. The crude aldehyde was then adhered to silica gel by mixing it with 1.5 weight equivalents silica gel (relative to the theoretical yield), dissolving it in  $CH_2Cl_2$  and removing the solvent *in vacuo* by rotary evaporation. A plug of silica was then assembled. This was done by adding 3-4 weight equivalents of silica (again relative to the theoretical yield) to a 300 mL coarse-porosity fritted glass funnel. An appropriately sized piece of filter paper relative to the size of the funnel was used to the top of the dry silica gel layer, and this layer was prewetted with hexanes. The dry packed

material was gently added evenly atop the filter paper. Another piece of appropriately sized filter paper was added atop this layer. The desired aldehyde was eluted off the plug via a 95:5 by volume mixture of Hex:EtOAc (3 column volumes), followed by 9:1 by volume mixture of Hex:EtOAc (3 column volumes). The solvent was removed *in vacuo* by rotary evaporation to afford the pure aldehyde (9.88 g, 74%) as clear, pale yellow oil.  $^1H$  NMR ( $CDCl_3$ , 400 MHz)  $\delta$  ppm 2.79 (t,  $J = 8.00$  Hz, 2 H) 2.97 (t,  $J = 7.60$  Hz, 2 H) 7.17-7.24 (m, 3 H) 7.30 (apparent triplet,  $J = 7.00$  Hz, 2 H) 9.83 (t,  $J = 1.46$  Hz, 1 H);  $^{13}C$  NMR ( $CDCl_3$ , 100 MHz)  $\delta$  ppm 28.4 ( $CH_2$ ) 45.5 ( $CH_2$ ) 126.6 (CH) 128.6 (CH) 128.9 (CH) 140.6 (C) 201.8 (C); GC-MS (EI) 134 ( $[M]^+$ , 61%) 133 ( $[M-1]^+$ , 10%) 105 (33%) 103 (16%) 92 (72%) 91 (100%) 78 (47%) 65 (16%).

**(E)-Methyl 5-phenylpent-2-enoate.**<sup>40</sup> The following procedure is a modification of the protocol outlined by Tius and co-workers.<sup>41</sup> To a 100 mL round-bottom flask equipped with a stir bar was added THF (16 mL), followed by dimethyl methoxycarbonylmethanephosphonate (8.01 g, 0.044 mol, 1.1 equiv). The flask was allowed to cool to  $0^\circ C$  in an ice water bath for 5 min. After this time, TMG (5.07 g, 0.044 mol, 1.1 equiv) was added to the flask dropwise over 5 min. The mixture was allowed to stir at  $0^\circ C$  for 30 min. After this time, the 3-phenylpropanal (5.37 g, 0.040 mol, 1 equiv) dissolved in 2.6 mL of THF was added dropwise rapidly, turning the solution bright yellow. After 5 min, the ice bath was removed and the solution was allowed to stir overnight at room temperature. After this time, the solution was quenched with 25 mL of deionized water. The solution was transferred to a separatory funnel and diluted with deionized water (100 mL) and  $Et_2O$  (100 mL). The phases were separated, and the aqueous layer was extracted with  $Et_2O$  ( $3 \times 50$  mL). The combined organic layers were washed with aqueous 1 M HCl ( $2 \times 100$  mL), deionized water (100 mL), and brine (150 mL). The organic layer was dried with sodium sulfate, and the solvent was removed *in vacuo* by rotary evaporation. The pure ester (6.00 g, 79%) was obtained as a clear, colorless oil.  $^1H$  NMR ( $CDCl_3$ , 400 MHz)  $\delta$  ppm 2.54 (apparent quartet,  $J = 7.50$  Hz, 2 H) 2.78 (t,  $J = 7.50$  Hz, 2 H) 3.73 (s, 3 H) 5.86 (dt,  $J = 15.67, 1.48$  Hz, 1 H) 7.02 (dt,  $J = 15.62, 6.86$  Hz, 1 H) 7.17-7.24 (m, 3 H) 7.30 (t,  $J = 7.20$  Hz, 2 H);  $^{13}C$  NMR ( $CDCl_3$ , 100 MHz)  $\delta$  ppm 34.1 ( $CH_2$ ) 34.6 ( $CH_2$ ) 51.7 ( $CH_3$ ) 121.7 (CH) 126.4 (CH) 128.6 (CH) 128.7 (CH) 141.0 (CH) 148.6 (C) 167.2 (C); GC-MS (EI) ( $[M]^+$ , %) 190 ( $[M]^+$ , 1%) 172 (5%) 144 (11%) 130 (9%) 117 (19%) 104 (46%) 91 (100%) 79 (10%) 77 (12%) 65 (21%) 57 (15%) 51 (12%) 39 (12%).

**(E)-5-Phenylpent-2-en-1-ol.**<sup>42</sup> To a flame-dried 1000 mL flask equipped with a large stir bar was added anhydrous  $Et_2O$  (350 mL) and  $LiAlH_4$  (1.14 g, 0.0336 mol, 1.12 equiv). The flask was sealed with a rubber septum and placed under a  $N_2$  atmosphere using an inlet needle. The mixture was cooled to  $0^\circ C$  in a large ice bath for 10 min, and after this time, anhydrous  $AlCl_3$  (1.51 g, 0.0113 mol, 0.377 equiv) was added rapidly to the flask. The solution was allowed to stir for 5 min and gradually transitioned from gray to white. At this time, (E)-methyl 5-phenylpent-2-enoate (5.71 g, 0.030 mol, 1 equiv) dissolved in 20 mL of anhydrous  $Et_2O$  was added to the flask over 5 min. After complete addition, the solution was allowed to stir at  $0^\circ C$  for 0.5 h.<sup>43</sup> After this time, the septum was removed and the solution was carefully quenched with 1 M HCl (200 mL). **Caution!** Large excess of hydrogen gas evolved. The biphasic solution was allowed to stir for 10 min, and gradually became clear. The quenched reaction mixture was transferred to a separatory funnel, and the phases were separated. The aqueous layer was extracted with  $Et_2O$  ( $2 \times 75$  mL), and the combined organic layers were washed with saturated aqueous  $NaHCO_3$  ( $2 \times 125$  mL), deionized water (125 mL), and brine (150 mL). The organic layer was dried with  $Na_2SO_4$ , and the solvent was removed *in vacuo* by rotary evaporation to give the pure alcohol **4b** (4.42 g, 91%) as a clear, colorless oil.  $^1H$  NMR ( $CDCl_3$ , 400 MHz)  $\delta$  ppm 1.29 (br. s, 1 H) 2.38 (apparent quartet,  $J = 7.40$  Hz, 2 H) 2.72 (apparent triplet,  $J = 8.20$  Hz, 2 H) 4.08 (t,  $J = 5.06$  Hz, 2 H) 5.62-5.79 (m, 2 H) 7.16-7.23 (m, 3 H) 7.29 (apparent triplet,  $J = 7.20$  Hz, 2 H);  $^{13}C$  NMR ( $CDCl_3$ , 100 MHz)  $\delta$  ppm 34.2 ( $CH_2$ ) 35.8 ( $CH_2$ ) 64.0 ( $CH_2$ ) 126.2 (CH) 128.6 (CH) 128.7 (CH) 129.9 (CH) 132.5 (CH) 142.0 (C); GC-MS (EI) 162 ( $[M]^+$ , 1%) 144 (32%) 108 (11%) 91 (100%) 65 (21%) 41 (12%).

(*E*)-(5-Methoxyprop-3-en-1-yl)benzene<sup>21</sup> (**7c**). Synthesis of (*E*)-(5-methoxyprop-3-en-1-yl)benzene, **7c**, (3.16 g, 90%) was accomplished using the procedure for the preparation of **7d** with the following modification: the reaction was conducted using (*E*)-5-phenylpent-2-en-1-ol (3.25 g, 0.025 mol). The ether **7c** was obtained as a clear, colorless oil. <sup>1</sup>H NMR (CDCl<sub>3</sub>, 500 MHz) δ ppm 2.42 (q, *J* = 7.30 Hz, 2 H) 2.75 (t, *J* = 8.17 Hz, 2 H) 3.33 (s, 2 H) 3.90 (d, *J* = 5.90 Hz, 2 H) 5.63 (dt, *J* = 15.44, 6.80 Hz, 1 H) 5.79 (dt, *J* = 15.44, 7.70 Hz, 1 H) 7.22 (d, *J* = 8.17 Hz, 3 H) 7.32 (t, *J* = 7.30 Hz, 2 H); <sup>13</sup>C NMR (CDCl<sub>3</sub>, 125 MHz) δ ppm 34.4 (CH<sub>2</sub>) 35.8 (CH<sub>2</sub>) 58.0 (CH<sub>3</sub>) 73.4 (CH<sub>2</sub>) 126.1 (CH) 127.1 (CH) 128.6 (CH) 128.7 (CH) 134.0 (CH) 142.0 (C); GC-MS (EI) 176 ([M]<sup>+</sup>, 0.1%) 144 (31%) 129 (20%) 115 (7%) 104 (4%) 91 (100%) 85 (15%) 71 (15%) 65 (23%) 56 (17%) 45 (14%).

**Reactions of Substrates with the Oxoammonium Salt 1a.**  
**Oxidation of 1-Fluoro-4-phenylbutan-2-ol (3n) to 1-Fluoro-4-phenylbutan-2-one (4n).** To a 100 mL round-bottom flask equipped with a stir bar were added the oxoammonium salt **1a** (11.15 g, 0.03716 mol, 2.5 equiv), 1-fluoro-4-phenylbutan-2-ol (2.50 g, 0.01486 mol, 1 equiv), 2,6 lutidine (3.58 g, 0.03344 mol, 2.25 equiv), and CH<sub>2</sub>Cl<sub>2</sub> (37.2 mL, 0.4 M in the alcohol). The flask was sealed with a rubber septum and stirred for 6 h. After this time, the solvent was removed *in vacuo* by rotary evaporation, affording a thick red residue. Anhydrous Et<sub>2</sub>O (≈100 mL) and pentane (100 mL) were added to the flask and allowed to stir for 10 min. This causes immediate precipitation of the nitroxide. *Note: It is imperative that the sides of the flask be scraped to ensure all the nitroxide precipitates out, releasing the product into solution.* The solids were saved for oxidant reclamation,<sup>44</sup> and the filtrate was then adhered to silica gel using 1.5 weight equivalents of SiO<sub>2</sub> (relative to the theoretical yield). The dry-packed material was gently added atop a silica gel plug. The plug was eluted with a 9:1 by volume mixture of Hex:EtOAc (2–3 column volumes). The solvent was removed *in vacuo* by rotary evaporation, affording the pure **4n** (1.54 g, 63%) as a clear, pale yellow oil. <sup>1</sup>H NMR (CDCl<sub>3</sub>, 400 MHz) δ ppm 2.87–2.94 (m, 2 H) 2.99 (apparent triplet, *J* = 7.70 Hz, 2 H) 4.79 (d, *J* = 47.59 Hz, 1 H) 7.25 (apparent triplet, *J* = 7.50 Hz, 3 H) 7.33 (apparent triplet *J* = 7.30 Hz, 2 H); <sup>13</sup>C NMR (CDCl<sub>3</sub>, 100 MHz) δ ppm 28.9 (d, *J*<sub>C-C-C-F</sub> = 1.8 Hz, CH<sub>2</sub>) 40.1 (CH<sub>2</sub>) 85.3 (d, *J*<sub>C-F</sub> = 184.9 Hz, CH<sub>2</sub>) 126.6 (CH) 128.6 (CH) 128.8 (CH) 140.7 (C) 206.3 (d, *J*<sub>C-C-F</sub> = 19.4 Hz, C); <sup>19</sup>F NMR (CDCl<sub>3</sub>, 377 MHz) δ ppm –230.79 (t, *J* = 47.70 Hz); GC-MS (EI) 166 ([M]<sup>+</sup>, 43%) 133 (44%) 115 (8%) 105 (82%) 91 (100%) 77 (28%) 65 (16%) 61 (6%) 51 (14%).

**Oxidation of 2,2-Difluoro-1-(*p*-tolyl)ethanol (3o) to 2,2-Difluoro-1-(*p*-tolyl)ethanone (4o).** 2,2-Difluoro-1-(*p*-tolyl)ethanone **4o** was obtained via the same protocol as **4n** with the following modification: the reaction was conducted using the 2,2-difluoro-1-(*p*-tolyl)ethanol **3o** (3.00 g, 0.01742 mol). The product (2.00 g, 68%) was obtained as a clear, pale yellow oil. <sup>1</sup>H NMR (CDCl<sub>3</sub>, 400 MHz) δ ppm 2.45 (s, 3 H) 6.27 (t, *J* = 53.62 Hz, 1 H) 7.33 (dd, *J* = 8.56, 0.58 Hz, 2 H) 7.98 (d, *J* = 8.17 Hz, 2 H); <sup>13</sup>C NMR (CDCl<sub>3</sub>, 100 MHz) δ ppm 22.2 (CH<sub>3</sub>) 111.5 (t, *J*<sub>C-F</sub> = 253.5 Hz, CF<sub>2</sub>H) 129.4 (t, *J*<sub>C-C-F</sub> = 1.5 Hz, C) 130.0 (CH) 130.0 (t, *J*<sub>C-C-C-F</sub> = 2.3 Hz, CH) 146.5 (C) 187.5 (t, *J*<sub>C-C-F</sub> = 25.4 Hz, C); <sup>19</sup>F NMR (CDCl<sub>3</sub>, 377 MHz) δ ppm –173.13 (d, *J* = 53.13 Hz); GC-MS (EI) 170 ([M]<sup>+</sup>, 4%), 119 (100%), 91 (82%), 89 (14%), 65 (32%), 63 (15%), 51 (17%), 39 (11%).

**Oxidation of (*E*)-(5-Methoxyprop-3-en-1-yl)benzene (7c) to (*E*)-5-Phenylpent-2-enal (8c).**<sup>45</sup> To a 250 mL round-bottom flask equipped with a stir bar were added the ether **7c** (1.763 g, 0.010 mol, 1 equiv), MeCN (67 mL), and deionized water (7 mL). After stirring for 5 min, the oxoammonium salt **1a** (3.301 g, 0.011 mol, 1.1 equiv) was added to the flask. The mixture was allowed to stir, and at the following times, 24, 47, 49, 68, and 72 h, was added an additional oxoammonium salt (0.600 g, 0.2 equiv) for a total of 1 additional equivalent. Reaction progress was monitored by <sup>1</sup>H NMR. After this time, the reaction was judged to be complete. At this time, the reaction mixture was diluted with water (30 mL) and transferred to a separatory funnel. The mixture was diluted with deionized water (50 mL) and Et<sub>2</sub>O (150 mL), and the layers were separated. The aqueous layer was extracted with Et<sub>2</sub>O (4 × 75 mL). The combined organic layers were washed with deionized water (2 × 100 mL) and brine (150 mL). The organic layer was dried with Na<sub>2</sub>SO<sub>4</sub>, and the solvent was removed *in vacuo* by rotary evaporation to give the crude aldehyde. The crude aldehyde was then adhered to silica gel by mixing it

with 1.5 weight equivalents silica gel (relative to the theoretical yield), dissolving it in CH<sub>2</sub>Cl<sub>2</sub> and removing the solvent *in vacuo* by rotary evaporation. A plug of silica was then assembled. This was done by adding 3–4 weight equivalents of silica (again relative to the theoretical yield) to a 150 mL coarse-porosity fritted glass funnel. An appropriately sized piece of filter paper relative to the size of the funnel was used to the top of the dry silica gel layer. The dry packed material was gently added evenly atop the filter paper. Another piece of appropriately sized filter paper was added over this layer. The desired aldehyde was eluted off the plug via a 9:1 by volume mixture of Hex:EtOAc (3 column volumes). The solvent was removed *in vacuo* by rotary evaporation to afford the pure aldehyde **8c** (0.641 g, 40%) as clear, bright yellow oil. <sup>1</sup>H NMR (CDCl<sub>3</sub>, 400 MHz) δ ppm 2.66–2.75 (m, 2 H) 2.87 (t, *J* = 7.80 Hz, 2 H) 6.16 (ddt, *J* = 15.64, 7.85, 1.47, 1.47 Hz, 1 H) 6.88 (dt, *J* = 15.63, 6.68 Hz, 1 H) 7.17–7.27 (m, 3 H) 7.30–7.37 (m, 2 H) 9.52 (d, *J* = 7.88 Hz, 1 H); <sup>13</sup>C NMR (CDCl<sub>3</sub>, 100 MHz) δ ppm 34.2 (CH<sub>2</sub>) 34.4 (CH<sub>2</sub>) 126.5 (CH) 128.5 (CH) 128.8 (CH) 133.5 (CH) 140.5 (C) 157.4 (CH) 194.1 (C); GC-MS (EI) 160 ([M]<sup>+</sup>, 1%) 116 (17%) 91 (100%) 65 (18%) 51 (7%) 39 (10%).

**Oxidation of (*E*)-(3-Methoxyprop-1-en-1-yl)benzene (7d) to Cinnamaldehyde (8d).** To a 250 mL round-bottom flask equipped with a stir bar were added the oxoammonium salt **1a** (10.804 g, 0.036 mol, 2.4 equiv), MeCN (67.5 mL), and deionized water (7.5 mL). After stirring for 5 min, (*E*)-(3-methoxyprop-1-en-1-yl)benzene **7d** (2.22 g, 0.015 mol, 1.0 equiv) was added to the flask. The mixture was allowed to stir for 8 h, and the reaction was judged to be complete after this time by <sup>1</sup>H NMR and GC analysis. The reaction mixture was diluted with water (30 mL) and Et<sub>2</sub>O (50 mL) and transferred to a separatory funnel. The mixture was additionally diluted with deionized water (50 mL) and Et<sub>2</sub>O (150 mL), and the layers were separated. The aqueous layer was extracted with Et<sub>2</sub>O (5 × 75 mL). The combined organic layers were washed with deionized water (2 × 100 mL) and brine (1 × 150 mL). The organic layer was dried with Na<sub>2</sub>SO<sub>4</sub>, and the solvent was removed *in vacuo* by rotary evaporation to give the crude aldehyde. The crude aldehyde was then adhered to silica gel by mixing it with 1.5 weight equivalents silica gel (relative to the theoretical yield), dissolving it in CH<sub>2</sub>Cl<sub>2</sub>, and removing the solvent *in vacuo* by rotary evaporation. A plug of silica was then assembled. This was done by adding 3–4 weight equivalents of silica (again relative to the theoretical yield) to a 150 mL coarse-porosity fritted glass funnel. An appropriately sized piece of filter paper relative to the size of the funnel was used to the top of the dry silica gel layer. The dry packed material was gently added evenly atop the filter paper. Another piece of appropriately sized filter paper was added over this layer. The desired aldehyde was eluted off the plug via a 9:1 by volume mixture of Hex:EtOAc (3 column volumes), followed by an 8:2 mixture of Hex:EtOAc (3 column volumes). The solvent was removed *in vacuo* by rotary evaporation to afford the pure aldehyde **8d** (1.51 g, 75%) as clear, bright yellow oil. <sup>1</sup>H NMR (CDCl<sub>3</sub>, 400 MHz) δ ppm 6.75 (dd, *J* = 15.97, 7.71 Hz, 1 H) 7.43–7.50 (m, 3 H) 7.52–7.64 (m, 3 H) 9.74 (d, *J* = 7.68 Hz, 1 H); <sup>13</sup>C NMR (CDCl<sub>3</sub>, 100 MHz) δ ppm 128.7 (CH) 128.8 (CH) 129.3 (CH) 131.4 (CH) 134.2 (C) 152.9 (CH) 193.8 (C); GC-MS (EI) 132 ([M]<sup>+</sup>, 58%) 131 (100%) 103 (62%) 77 (51%) 63 (12%) 51 (38%).

**Oxidative Functionalization of Cycloheptatriene: Tropylacetylacetone.**<sup>47</sup> To a 100 mL round-bottom flask equipped with a stir bar were added the oxoammonium salt **1a** (3.58 g, 0.01085 mol, 2.0 equiv) and MeCN (30 mL). Cycloheptatriene (0.50 g, 0.00543 mol, 1 equiv) was added dropwise to this solution. After 4 h, the conversion was checked by NMR. Once confirmed to be completely oxidized, acetylacetone (0.544 g, 0.00543 mol, 1 equiv) was added dropwise to the flask, followed by pyridine (0.429 g, 0.00543 mol, 1 equiv). The reaction was allowed to stir overnight. After this time, the reaction was quenched with water (30 mL). The mixture was transferred to a separatory funnel. The aqueous layer was extracted with a 7:3 by volume mixture of Hexanes:EtOAc (3 × 70 mL).<sup>48</sup> The combined organic layers were washed with 1 M HCl (2 × 50 mL) and brine (1 × 150 mL). The organic layer was dried with Na<sub>2</sub>SO<sub>4</sub>, and the solvent was removed *in vacuo* by rotary evaporation to afford a pale yellow solid. This initial solid was washed with a minimal amount of pentane, and the pentane was decanted off. The solid was dried *in vacuo* to afford the pure **18** (0.785 g,



76%) as a white solid (mp 123–124 °C). <sup>1</sup>H NMR (CDCl<sub>3</sub>, 500 MHz) δ ppm 2.18 (s, 6 H) 2.92 (dt, *J* = 11.35, 6.80 Hz, 1 H) 4.01 (d, *J* = 11.35 Hz, 1 H) 5.18 (dd, *J* = 9.31, 6.59 Hz, 2 H) 6.27 (dt, *J* = 9.31, 3.07 Hz, 2 H) 6.71 (t, *J* = 3.18 Hz, 2 H); <sup>13</sup>C NMR (CDCl<sub>3</sub>, 100 MHz) δ ppm 29.8 (CH<sub>3</sub>) 38.4 (CH) 70.2 (CH) 122.1 (CH) 126.7 (CH) 131.4 (CH) 203.3 (C); GC–MS (EI) 194 ([M]<sup>+</sup>, 0.1%) 147 (58%) 129 (15%) 105 (16%) 103 (11%) 91 (87%) 77 (18%) 65 (15%) 51 (11%) 43 (100%) 39 (11%).

**Relative Reactivity Protocols. Procedure for Relative Reactivity Study under Unassisted Conditions.** In a vial equipped with a stir bar were added benzyl alcohol (0.108 g, 1 equiv), a competing alcohol (1 equiv), and CH<sub>2</sub>Cl<sub>2</sub> (5 mL). To this was added **1a** (0.600 g, 2.0 equiv), and the mixture was allowed to stir for 12 h. An aliquot of the crude now-completed oxidation mixture was obtained and analyzed by <sup>1</sup>H NMR. Integration of the representative peaks of benzyl alcohol and the competing alcohol and/or of their corresponding carbonyl species was used to obtain the relative reactivities by the ratio of the peaks. Experimentally derived reactivities are noted in the paper.

**Procedure for Relative Reactivity Study under Base-Assisted Conditions.** In a vial equipped with a stir bar were added benzyl alcohol (0.108 g, 1 equiv), a competing alcohol (1 equiv), and CH<sub>2</sub>Cl<sub>2</sub> (5 mL). To this mixture was added 2,6-lutidine (0.225 g, 2.1 equiv), and the subsequent mixture was allowed to stir for 5 min. After this time, **1a** (0.600 g, 2.0 equiv) was added, and the mixture was allowed to stir for 12 h. An aliquot of the crude now-completed oxidation mixture was obtained and analyzed by <sup>1</sup>H NMR. Integration of the representative peaks of benzyl alcohol and the competing alcohol and/or of their corresponding carbonyl species was used to obtain the relative reactivities by the ratio of the peaks. Experimentally derived reactivities are noted in the paper.

## ■ ASSOCIATED CONTENT

### ● Supporting Information

<sup>1</sup>H, <sup>13</sup>C, and <sup>19</sup>F NMR spectra of the compounds are presented. Energies and Cartesian coordinates are provided for all stationary points as well as intrinsic reaction coordinate experiments. The Supporting Information is available free of charge on the ACS Publications website at DOI: 10.1021/acs.joc.5b01240.

## ■ AUTHOR INFORMATION

### Corresponding Author

\*E-mail: nicholas.leadbeater@uconn.edu.

### Author Contributions

<sup>†</sup>These authors contributed equally to this work.

### Notes

The authors declare no competing financial interest.

## ■ ACKNOWLEDGMENTS

This work was supported by the National Science Foundation (CAREER Award CHE-0847262) (T.A.H., C.B.K., R.J.W., N.E.L.), the University of Connecticut Office of Undergraduate Research (J.M.O., R.J.W.) and Holster Scholars First-Year Project (J.M.O.), and by Stonehill College (L.J.T., R.J.W.). We would like to thank Dr. Christian Hamann of Albright College for assistance throughout the project. We would also like to thank Drs. James M. Bobbitt, Robert R. Birge, and José A. Gascón of the University of Connecticut for helpful discussions.

## ■ REFERENCES

(1) (a) Smith, M. B.; March, J. *March's Advanced Organic Chemistry*, 5th ed.; J. W. Wiley: New York, 2001. (b) Bäckvall, J.-E., Ed. *Modern Oxidation Methods*; WILEY-VCH: Weinheim, 2004. (c) Trost, B. M.; Fleming, I. *Comprehensive Organic Synthesis: Selectivity, Strategy, and Efficiency in Modern Organic Chemistry*; Pergamon Press: Oxford, U.K., 1991. (d) Caron, S. *Practical Synthetic Organic Chemistry: Reactions, Principles, and Techniques*; WILEY-VCH: Weinheim, 2011.

(2) Reviews on TEMPO-based oxidants and example oxidations: (a) Vogler, T.; Studer, A. *Synthesis* **2008**, 2008, 1979–1993. (b) Bobbitt, J. M.; Brückner, C.; Merbouh, N. *Org. React.* **2009**, 74, 103–424. (c) Montanari, F.; Quici, S.; Henry-Riyad, H.; Tidwell, T. T.; Studer, A.; Vogler, T. 2,2,6,6-Tetramethylpiperidin-1-oxyl. In *Encyclopedia of Reagents for Organic Synthesis*; John Wiley & Sons: New York, 2007. (d) Hoover, J. M.; Stahl, S. S. *J. Am. Chem. Soc.* **2011**, 133, 16901–16910. (e) Garcia-Mancheño, O.; Stopka, T. *Synthesis* **2013**, 45, 1602–1611.

(3) Examples of other nitroxides and their uses: (a) Iwabuchi, Y. *Chem. Pharm. Bull.* **2013**, 61, 1197–1213. (b) Shibuya, M.; Nagasawa, S.; Osada, Y.; Iwabuchi, Y. *J. Org. Chem.* **2014**, 79, 10256–10268. (c) Shibuya, M.; Tomizawa, M.; Sasano, Y.; Iwabuchi, Y. *J. Org. Chem.* **2009**, 74, 4619–4622. (d) Likhtenshtein, G. I.; Yamauchi, J.; Nakatsuji, S.; Smirnov, A. I.; Tamura, R. *Nitroxides*; Wiley-VCH: Weinheim, Germany, 2008.

(4) Information on TEMPO-based oxoammonium salts and some of their reactions relevant to this paper: (a) Leadbeater, N. E.; Bobbitt, J. M. *Aldrichimica Acta* **2014**, 47, 65–74. (b) Mercadante, M. A.; Kelly, C. B.; Bobbitt, J. M.; Tilley, L. J.; Leadbeater, N. E. *Nat. Protoc.* **2013**, 8, 666–676. (c) Kelly, C. B. *Synlett* **2013**, 24, 527–528. (d) Bobbitt, J. M.; Merbouh, N. *Org. Synth.* **2005**, 82, 80–86. (e) Richter, H.; Fröhlich, R.; Daniliuc, C.-G.; García Mancheño, O. *Angew. Chem., Int. Ed.* **2012**, 51, 8656–8660. (f) Rohlmann, R.; Stopka, R.; Richter, H.; García Mancheño, O. *J. Org. Chem.* **2013**, 78, 6050–6064. (g) Lackner, A. D.; Samant, A. V.; Toste, F. D. *J. Am. Chem. Soc.* **2013**, 135, 14090–14093. (h) Richter, H.; García Mancheño, O. *Org. Lett.* **2011**, 13, 6066–6069. (i) Richter, H.; Rohlmann, R.; García Mancheño, O. *Chem. - Eur. J.* **2011**, 17, 11622–11627. (j) Wertz, S.; Kodama, S.; Studer, A. *Angew. Chem., Int. Ed.* **2011**, 50, 11511–11515.

(5) Information on other oxoammonium salts and their reactions: (a) Cao, Q.; Dorman, L. M.; Rogan, L.; Hughes, N. L.; Muldoon, M. J. *Chem. Commun.* **2014**, 50, 4524–4543. (b) Wertz, S.; Studer, S. *Green Chem.* **2013**, 15, 3116–3134. (c) Rychnovsky, S. D.; Beauchamp, T.; Vaidyanathan, R.; Kwan, T. *J. Org. Chem.* **1998**, 63, 6363–6374. (d) Rychnovsky, S. D.; McLernon, T. L.; Rajapakse, H. J. *Org. Chem.* **1996**, 61, 1194–1195. (e) Tanaka, H.; Kawakami, Y.; Goto, K.; Kuroboshi, M. *Tetrahedron Lett.* **2001**, 42, 445–448. (f) Shibuya, M.; Tomizawa, M.; Sasano, Y.; Iwabuchi, Y. *J. Org. Chem.* **2009**, 74, 4619–4622. (g) Hayashi, M.; Shibuya, M.; Iwabuchi, Y. *Org. Lett.* **2012**, 14, 154–157. (h) Kelly, C. B.; Mercadante, M. A.; Hamlin, T. A.; Fletcher, M. H.; Leadbeater, N. E. *J. Org. Chem.* **2012**, 77, 8131–8141. (i) Hamlin, T. A.; Kelly, C. B.; Leadbeater, N. E. *Eur. J. Org. Chem.* **2013**, 2013, 3658–3661.

(6) (a) Ciriminna, R.; Pagliaro, M. *Org. Process Res. Dev.* **2010**, 14, 245–251. (b) Caron, S.; Dugger, R. W.; Ruggeri, S. G.; Ragan, J. A.; Ripin, D. H. B. *Chem. Rev.* **2006**, 106, 2943–2989. (c) Dugger, R. W.; Ragan, J. A.; Ripin, D. H. B. *Org. Process Res. Dev.* **2005**, 9, 253–258.

(7) Semmelhack, M. F.; Schmid, C. R.; Cortés, D. A. *Tetrahedron Lett.* **1986**, 27, 1119–1122.

(8) Bobbitt, J. M.; Bartelson, A. L.; Bailey, W. F.; Hamlin, T. A.; Kelly, C. B. *J. Org. Chem.* **2014**, 79, 1055–1067.

(9) Bailey, W. F.; Bobbitt, J. M.; Wiberg, K. B. *J. Org. Chem.* **2007**, 72, 4504–4509.

(10) Frisch, M. J.; Trucks, G. W.; Schlegel, H. B.; Scuseria, G. E.; Robb, M. A.; Cheeseman, J. R.; Scalmani, G.; Barone, V.; Mennucci, B.; Petersson, G. A.; Nakatsuji, H.; Caricato, M.; Li, X.; Hratchian, H. P.; Izmaylov, A. F.; Bloino, J.; Zheng, G.; Sonnenberg, J. L.; Hada, M.; Ehara, M.; Toyota, K.; Fukuda, R.; Hasegawa, J.; Ishida, M.; Nakajima, T.; Honda, Y.; Kitao, O.; Nakai, H.; Vreven, T.; Montgomery, J. A., Jr.; Peralta, J. E.; Ogliaro, F.; Bearpark, M.; Heyd, J. J.; Brothers, E.; Kudin, K. N.; Staroverov, V. N.; Kobayashi, R.; Normand, J.; Raghavachari, K.; Rendell, A.; Burant, J. C.; Iyengar, S. S.; Tomasi, J.; Cossi, M.; Rega, N.; Millam, J. M.; Klene, M.; Knox, J. E.; Cross, J. B.; Bakken, V.; Adamo, C.; Jaramillo, J.; Gomperts, R.; Stratmann, R. E.; Yazyev, O.; Austin, A. J.; Cammi, R.; Pomelli, C.; Ochterski, J. W.; Martin, R. L.; Morokuma, K.; Zakrzewski, V. G.; Voth, G. A.; Salvador, P.; Dannenberg, J. J.; Dapprich, S.; Daniels, A. D.; Farkas, Ö.; Foresman, J. B.; Ortiz, J. V.; Cioslowski, J.;

Fox, D. J. *Gaussian 09*, Revision A.02; Gaussian, Inc.: Wallingford, CT, 2009.

(11) (a) Barone, V.; Cossi, M. *J. Phys. Chem. A* **1998**, *102*, 1995–2001. (b) Barone, V.; Cossi, M.; Tomasi, J. *J. Comput. Chem.* **1998**, *19*, 404–417.

(12) (a) Becke, A. D. *J. Chem. Phys.* **1993**, *98*, 5648–5652. (b) Lee, C.; Yang, W.; Parr, R. G. *Phys. Rev. B: Condens. Matter Mater. Phys.* **1988**, *37*, 785–789. (c) Vosko, S. H.; Wilk, L.; Nusair, M. *Can. J. Phys.* **1980**, *58*, 1200–1211. (d) Stephens, P. J.; Devlin, F. J.; Chabalowski, C. F.; Frisch, M. J. *J. Phys. Chem.* **1994**, *98*, 11623–11627.

(13) (a) Ditchfield, R.; Hehre, W. J.; Pople, J. A. *J. Chem. Phys.* **1971**, *54*, 724. (b) Hehre, W. J.; Ditchfield, R.; Pople, J. A. *J. Chem. Phys.* **1972**, *56*, 2257. (c) Hariharan, P. C.; Pople, J. A. *Theor. Chim. Acta.* **1973**, *28*, 213–222.

(14) Hay, P. J.; Wadt, W. R. *J. Chem. Phys.* **1985**, *82*, 270–283.

(15) Cao, X. Y.; Dolg, M. *J. Mol. Struct.: THEOCHEM* **2002**, *581*, 139–147.

(16) (a) Fukui, K. *Acc. Chem. Res.* **1981**, *14*, 363–368. (b) Hratchian, H. P.; Schlegel, H. B. In *Theory and Applications of Computational Chemistry: The First 40 Years*; Dykstra, C. E., Frenking, G., Kim, K. S., Scuseria, G., Eds.; Elsevier: Amsterdam, 2005.

(17) Legault, C. Y. *CYLview, 1.0b*; Université de Sherbrooke: Sherbrooke, Québec, Canada, 2009. <http://www.cylview.org>.

(18) Lambert, K. M.; Bobbitt, J. M.; Eldirany, S. A.; Wiberg, K. M.; Bailey, W. F. *Org. Lett.* **2014**, *16*, 6484–6487.

(19) Pradhan, P. A.; Bobbitt, J. M.; Bailey, W. F. *J. Org. Chem.* **2009**, *74*, 9524–9527.

(20) As part of a separate study, we prepared a 2-(benzyloxy) benzaldehyde-derived trifluoromethyl ketone *via* the oxidation of the corresponding CF<sub>3</sub> carbinol with **1a**. Only trace oxidative debenzoylation was observed in this case despite the electron deficient nature of  $\alpha$ -CF<sub>3</sub> alcohols, thus implying that oxidation of phenyl ethers is very difficult.

(21) Kelly, C. B.; Ovian, J. M.; Cywar, R. M.; Gosselin, T. R.; Wiles, R. J.; Leadbeater, N. E. *Org. Biomol. Chem.* **2015**, *13*, 4255–4259.

(22) Richter, H.; García-Mancheño, O. *Eur. J. Org. Chem.* **2010**, 4460–4467.

(23) Kelly, C. B.; Lambert, K. M.; Mercadante, M. A.; Ovian, J. M.; Bailey, J. F.; Leadbeater, N. E. *Angew. Chem., Int. Ed.* **2015**, *54*, 4241–4245.

(24) For information on the tropylium ion, see: (a) Kane, J. L.; Danheiser, R. L. *Tropylium Tetrafluoroborate in Encyclopedia of Reagents for Organic Synthesis*; John Wiley & Sons: New York, 2001. (b) von E. Doering, W. v. E.; Knox, L. H. *J. Am. Chem. Soc.* **1954**, *76*, 3203–3206. (c) Pietra, F. *Chem. Rev.* **1973**, *73*, 293–364.

(25) Allen, J. M.; Lambert, T. H. *J. Am. Chem. Soc.* **2011**, *133*, 1260–1262.

(26) Breton, T.; Liaigre, D.; Belgsir, E. M. *Tetrahedron Lett.* **2005**, *46*, 2487–2490.

(27) Conrow, K. *J. Am. Chem. Soc.* **1959**, *81*, 5461–5467.

(28) Pradhan, P. P.; Bobbitt, J. M.; Bailey, W. F. *Org. Lett.* **2006**, *8*, 5485–5487.

(29) This observation is even consistent with the fact that the most common preparative route to synthesis of tropylium tetrafluoroborate is the oxidation of cycloheptatriene using the trityl cation prepared *in situ* by treatment of triphenylmethanol with tetrafluoroboric acid. This directly implies that the trityl cation is a stronger oxidant than cycloheptatriene and, therefore, would be more resistant to oxidation when treated with oxoammonium cations.

(30) Ravikumar, I.; Saha, S.; Ghosh, P. *Chem. Commun.* **2011**, 47, 4721–4723.

(31) Grassi, D.; Li, H.; Alexakis, A. *Chem. Commun.* **2012**, 48, 11404–11406.

(32) Kitazume, T.; Asai, M.; Lin, J. T.; Yamazaki, T. *J. Fluorine Chem.* **1987**, *35*, 477–488.

(33) Prakash, G. K. S.; Hu, J.; Olah, G. A. *J. Fluorine Chem.* **2001**, *112*, 355–360.

(34) Kaneko, S.; Yamazaki, T.; Kitazume, T. *J. Org. Chem.* **1993**, *58*, 2302–2312.

(35) Matsubara, R.; Jamison, T. F. *J. Am. Chem. Soc.* **2010**, *132*, 6880–6881.

(36) NaH was prewashed with pentane five times prior to use to remove the mineral oil. The now whitish solid was dried under light vacuum.

(37) The alkylation process can be dramatically accelerated by heating to 40–45 °C without any detrimental effects.

(38) Henderson, W. H.; Check, C. T.; Proust, N.; Stambuli, J. P. *Org. Lett.* **2010**, *12*, 824–827.

(39) Jana, R.; Tunge, J. A. *Org. Lett.* **2009**, *11*, 971–974.

(40) Poeylout-Palena, A. A.; Testero, S. A.; Mata, E. G. *J. Org. Chem.* **2008**, *73*, 2024–2027.

(41) Barrow, R. A.; Hemscheidt, T.; Liang, J.; Paik, S.; Moore, R. E.; Tius, M. A. *J. Am. Chem. Soc.* **1995**, *117*, 2479–2490.

(42) Race, N. J.; Bower, J. F. *Org. Lett.* **2013**, *15*, 4616–4619.

(43) It is imperative that the reaction mixture be quenched 30 min after addition of the ester. Longer reaction times lead to unwanted over reduction of the double bond.

(44) Regeneration of the oxoammonium salt **1a** from the nitroxide **1b** can be performed as outlined in our published protocol; see ref 4b. It is recommended that the nitroxide be recrystallized from EtOAc first to remove lutidinium tetrafluoroborate salt.

(45) Schmidt, A.; Hilt, G. *Org. Lett.* **2013**, *15*, 2708–2711.

(46) Park, C. P.; Kim, D.-P. *J. Am. Chem. Soc.* **2010**, *132*, 10102–10106.

(47) Komatsu, K.; Tanaka, S.; Saito, S.; Okamoto, K. *Bull. Chem. Soc. Jpn.* **1977**, *50*, 3425–3426.

(48) On the basis of solubility experiments, we found this to be the optimal solvent ratio for extraction that minimized impurity solubility (**1d** tetrafluoroborate, MeCN, etc.) while maximized the solubility of **18**.